30,000 Years of the southwestern Lake Urmia (Iran) paleoenvironmental evolution inferred from mineralogical indicators from lake and watershed sediments

Ting Kong, Alina Tudryn, Elisabeth Gibert-Brunet, Piotr Tucholka, Seyed-Hani Motavalli-Anbaran, Hesam Ahmady-Birgani, Mohammad Lankarani, Serge Miska, Aurélie Noret, Olivier Dufaure

30,000 Years of the southwestern Lake Urmia (Iran) paleoenvironmental evolution inferred from mineralogical indicators from lake and watershed sediments

Ting Kong [a, *], Alina Tudryn [a], Elisabeth Gibert-Brunet [a], Piotr Tucholka [a], Seyed-Hani Motavalli-Anbaran [b], Hesam Ahmady-Birgani [c], Mohammad Lankarani [d], Serge Miska [a], Aurélie Noret [a], Olivier Dufaure [a]

[a] University Paris-Saclay, CNRS, UMR 8148-GEOPS, 91405, Orsay, France
[b] Institute of Geophysics, University of Tehran, Tehran, Iran
[c] Faculty of Natural Resources, Urmia University, Urmia, Iran
[d] School of Geology, University-College of Science, University of Tehran, Tehran, Iran

Abstract

In order to understand the evolution of Lake Urmia (Iran), one of the largest terminal lakes in Western Asia before its level drop over the past two decades, two sediment cores (Golman 6, 8.0 m; Golman 7, 12.5 m) were collected from the recently dried-out southwestern part of the lake. These sediment cores represent a continuous sedimentary sequence, composite core, that was extensively studied for grain size, total mineralogy including clay minerals, carbonates and their crystallinities, in comparison with the basin geological formations and within a reliable AMS-^{14}C time scale. Lake Urmia deposits cover the time-span from 30 to ca 2 cal kyr BP. Grain-size of the siliclastic fractions from the lower part of the composite core consists of fine-silt and clay particles likely representing lacustrine deposits while the top sediments are characterized by variable composition of sand and silt. At about 30 cal kyr BP, our proxies indicate a low lake stand and even drying out at the coring site, which was followed by water level rise and the establishment of lacustrine conditions between 29.85 and 20.21 cal kyr BP. Since then, all our data suggest lake's highly unstable conditions. Subsequently, clearly low lake levels to sometimes the drying out was

recorded during the 20.21-15.33 cal kyr BP, 13.27-11.82 cal kyr BP and 5.64-4.10 cal kyr BP intervals. In contrast, lacustrine conditions were re-established between 15.33 and 13.27 cal kyr BP, between 11.82 and 5.64 cal kyr BP and between 4.10 and 2.34 cal kyr BP. High water level recorded between 15.33 and 13.27 cal kyr BP can be attributed to the Bölling/Alleröd warming, and the following regressive phase during the 13.27-11.82 cal kyr BP period corresponds to the Younger Dryas period. In the Early-Mid Holocene, the lacustrine environment from 11.82 to 5.64 cal kyr BP was characterized by high aragonite and salt contents, highlighting evaporative environment as like during the 29.85-20.21 cal kyr BP period. Our results allowed the Late Quaternary climate reconstruction at Lake Urmia basin scale and record the past climate change at a larger Western Asia scale.

Keywords: Lake Urmia; Late Quaternary palaeoenvironments; Water level change; Carbonates; Clay minerals, ^{14}C dating

1. Introduction

Located in Northwestern Iran, Lake Urmia is a natural habitat of brine shrimp *Artemia urmiana* and the salinity of lake water commonly ranges from 120 to 280 $g.L^{-1}$, regarded as a UNESCO biosphere reserve and a Ramsar wetland (Asem *et al.*, 2012). However, since increased anthropic activities inside the lake basin (brine shrimp farming) and its watershed area (agriculture) in the mid-1990s, Lake Urmia dropped by 7 m, that led to drastic reduction in lake surface area, ground- and lake water salinization, desertification and dust storms threatening health conditions of millions of people at a regional scale (Alipour, 2006; Pengra, 2012; Ghalibaf and Moussavi, 2014; AghaKouchak *et al.*, 2015; Ahmady-Birgani *et al.*, 2015; Ahmady-Birgani *et al.*, 2020). The decline of the lake water volume has already concentrated the original salinity even up to 380 $g.L^{-1}$ in many locations (Sharifi *et al.*, 2018). The water-level drop has been

attributed to anthropogenic causes such as the construction of many dams on rivers feeding the lake, abusive groundwater abstraction, and to rainfall declining (Alipour, 2006; Jalali *et al.*, 2016), although the exact impact of both factors is not yet well identified. Even if the anthropogenic causes can be estimated and modified, the past evolution of the lake basin that may help to better understand the ongoing and future lakes evolutions is not well known through some data already existed. Asem et al. (2012) mentioned historical documents indicating that Lake Urmia experienced a severe drought in the beginning of the 1800 ’s with a maximum lake depth of 75 cm and an east-west road created across the lakebed. Existing studies of Late Quaternary sediments from the lake including sedimentology, geochemistry and pollen, are various but (i) concern only the most recent Holocene period about the last 2550 years (Talebi *et al.*, 2016) or surface sediments (Erfan *et al.*, 2017; Sharifi *et al.*, 2018), (ii) focus on the whole Holocene but with a low temporal resolution (Bottema, 1986; Kelts and Shahrabi, 1986), (iii) on Late Pleistocene and the Holocene without precise chronology (Mirzapour *et al.*, 2021a; Mirzapour *et al.*, 2021b), or (iv) cover large time scale (200 kyr) but again with poor or missing information on Late Pleistocene and the Holocene (Djamali *et al.*, 2008a; Djamali *et al.*, 2008b; Stevens *et al.*, 2012). Whatever their chronological resolution, these studies indicate the highest amplitude of lake-level variations at a glacial-interglacial time scale with a dry open mountain steppe dominating during the glacial periods and a steppe-forest environment during interglacials. Over the Holocene, saline deposition seems almost continuous with clear water level changes but no visible total desiccation of the lake. In addition, the vegetation reached its maximum destruction due to increasing human impact during the last centuries.

The present study aims to accurately decipher the pattern and trends of environmental change in the southwestern part of the lake basin over 30 kyr. Preliminary results on Lake Urmia sedimentary cores were published by our team (Tudryn *et al.*, 2021), proposing the lake level fluctuations but with an overall unclear timescale. In order to reliably precise the chronology and the related environment phases, we performed mineralogical studies both on the core sediments and on those of the Shahr Chay River catchment, which

is the main provider of detrital input to the coring site. Based on X-ray diffraction analyses on bulk sediment samples, we identified the principal silicates, carbonates and evaporites, on clayish fraction - clay minerals, and we analyzed sediment grain size distribution. The chronology has been established on 13 ^{14}C dating of organic matter and authigenic carbonates.

2. Study area

Lake Urmia basin (35.5–38.5° N and 44–48° E) is part of the tectonic crush zone between the colliding Arabian and Eurasian plates (McKenzie, 1976) (Fig. 1a). Based on Sharifi and co-authors (2018), the lacustrine basin is divided into two sub-basins: the deep northern basin and the shallow southern basin with an average depth of 10 and 2 m respectively. Between two basins, an east-west dike-type highway that stretches 15 km across the center of the lake has been constructed. The whole lake has 13 perennial and seasonal tributaries, but the main water inflow to the southwestern lake area close to the coring site originates from Shahr Chay River that is also named Shahi Chay River (Sharifi *et al.*, 2018). Sharifi and co-authors (2018) also report the annual mean river discharge and the mean catchment area of the major tributaries. Lake Urmia displays a unique, highly valuable biodiversity that favors a highly productive agriculture and brine shrimp farming, and makes the region as one of the most important economic poles of Iran.

The geology of Lake Urmia catchment is quite diverse, ranging from Precambrian metamorphic complexes to Quaternary mud deposits (Fig. 1b). In the east and northeast parts of the catchment, volcanic and volcano-sedimentary formations dominate while intrusive rocks prevail over the rest of the catchment, with mainly metamorphic rocky outcrops in the Zagros to the west, complemented in the south by dolomites, sandstones, quartz and volcanic rocks from the Infracambrian. Carbonate rocks are found in south and western parts of the basin while evaporative sedimentary units are only found northeast of the watershed.

Owing to the effects of local topography, the Urmia basin climate is mainly controlled by the surrounding mountains, and thus the semi-arid continental climate is characterized by rather large variations in temperature and precipitation. According to the Urmia meteorological station (west of Urmia Lake at 1,313 m a.s.l.), the temperature was below 10 ℃ in winter and up to 40 ℃ in summer, and the mean annual precipitation was recorded as about 300 mm (Kelts and Shahrabi, 1986; Sharifi *et al.*, 2018). Whereas a steady decline is registered since several years, the most recent satellite altimeter data indicating a drop of approximately 7 m over the last 20 years, with a lake level ranging from 1277.5 m in 1999 to 1270.85 m in 2019 (Ahmady-Birgani *et al.*, 2020). Because the southern part of the lake (south of the dike-type highway) is relatively shallow, the water level decline exacerbates the dramatic decline of the lake surface area. According to Ahmady-Birgani et al.(2020), the lake surface decreases all the time and from 1999 to 2019, the lake even lost half of its surface area (5000 km^2 in 1999 vs 2400 km^2 in 2019) and had less of almost 20 bm^3 of its water volume.

3. Materials and methods

3.1. Material collection

3.1.1. Lake sediment sampling

In September 2017, two sediment cores, i.e. Golman 6 (8.0 m long) and Golman 7 (12.5 m long), have been collected from the SW part of recently dried out part of the lake, near the city of Urmia (Fig. 1c, Table 1). The cores have been taken in close proximity to each other, with the mechanic corer and a borehole casing at a distance from today's shoreline allowing safe use of the corer. Details of sampling and coring conditions are given in Tudryn et al. (2021). The coring was stopped when pressurized water with mud and gas with

an intense H_2S odor rose up from the Golman 7 borehole to the lake surface and when gas with the same odor rose up from the Golman 6 borehole.

Due to the presence of interbedded captured water (either residual water from the sediment or ancient lake water trapped within the deposits), the 4.2 to 8.65 m section of Golman 7 core was too humid to be retrieved by the corer, leading to an empty section for this depth interval. Moreover, consequently to the soft and humid lacustrine ground at the core site, the first section of Golman 6 core taken from 0 m to 4.0 m depth, was compacted and only collected as 3.15-4.0 m depth. Although the two cores Golman 6 and Golman 7 present these inconsistencies, they represent together a continuous sequence as a composite core (Fig. 2a, b, c).

3.1.2. Catchment sediment sampling

In June 2021, eight geological samples have been collected from the catchment area of the Shahr Chay River that is the major supplier of detrital material into the lake at the coring location. These 8 samples have been selected according to the main geological formations of the river catchment (Table 1, Fig. 1c). Accordingly, samples represent the following formations: 1- pyroclastic and claystone with vertebrate fauna remains, andesitic to basaltic volcanics; 2 and 7- high level piedmont fan and valley terraces deposits; 3, 4 and 5-red beds composed of red conglomerate, sandstone, marl, gypsiferous marl; 6 - phyllite, slate and meta-sandstone (Hamadan phyllites); 8 - dark gray medium- bedded to massive limestone.

3.2. Methods

3.2.1. Grain size and clay mineralogy

Grain size and clay mineral analyses have been performed at the GEOPS laboratory, Paris-Saclay University (Orsay, France) on 116 and 84 samples taken at every 5 cm depth intervals from cores Golman

7 and Golman 6 respectively. For each sample, about 5-10 g of air-dried, disaggregated sediment was pre-treated in a 33% hydrogen peroxide (H_2O_2) bath to remove organic matter and then with a 20% acetic acid solution (CH_3COOH) to remove carbonates. After that, the samples were rinsed with deionized water in order to obtain neutral pH. These organic-free and carbonate-free samples have then been used for grain size distribution and for clay mineral analyses. The grain-size distribution was carried out on samples dispersed by ultrasonic vibrator for 3 min before analysis using a Malvern Mastersizer 2000 laser device.

Clay minerals have been identified by X-ray diffraction (XRD) on oriented mounts of clay sized (< 2 μm) particles with a PANalytical diffractometer, following the laboratory routine of the GEOPS laboratory. Three XRD runs were made, after a specific chemical treatment of air-drying, ethylene glycol solute leaching for 12 h, and heating at 500 °C for 2 h and return back to normal temperature (Holtzapffel, 1985). The identification of clay minerals peaks was made mainly according to the position of the (001) series of basal reflections. Semi-quantitative estimates of peak areas of the basal reflections for the main clay mineral groups of smectite (including mixed-layers) (16.9 Å), illite (10 Å), kaolinite (3.57 Å), chlorite (3.54 Å) and kaolinite + chlorite (7.16 Å) were carried out on the glycolated curve using the MacDiff software (Petchick, 2000). Relative proportions of kaolinite and chlorite were determined based on the ratio 3.57/3.54 Å of the peak areas. Evaluation of each clay mineral has an accuracy of ca 5%. Furthermore, the illite chemistry index was estimated using the ratio of the integrated 5 Å and 10 Å illite peak areas on the XRD diffractograms (Esquevin, 1969). The illite chemistry index value > 0.4 represents the Al-rich illites, while a value < 0.4 represents Fe- and Mg- rich illites (Diekmann *et al.*, 1996; Ehrmann *et al.*, 2005). Additionally, the illite and smectite crystallinities were separately obtained from the full width half maximum (FWHM) of the 10 Å and 16.9 Å peak respectively. According to Ehrmann et al. (2005), this parameter indicates the state of illite crystallization as (i) very well crystallized (< 0.4), well crystallized (0.4-0.6), moderately crystallized (0.6-0.8), poorly crystallized (>0.8), and of (ii) smectite as well crystallized (<1.5), moderately crystallized (1.5-2.0), and poorly crystallized (>2.0) (Ehrmann *et al.*, 2005).

3.2.2. Bulk sediment mineralogy

Identification of total mineralogical components of the whole sediment has been performed by XRD at GEOPS laboratory by XRD analyses of 52 samples with an X'Pert Pro PANalytical diffractometer, Cu-K source, 2Θ range 5°-80°, 4 h runs. The identification of mineralogical phases was conducted using the PANalytical HighScore software with crystallography open database and ICDD PDF-4/Minerals database following the laboratory routine at GEOPS laboratory. The semi quantification of minerals was determined according to the area of main peak on quartz (3.34 Å). In addition, specific carbonates have been identified through analyzes during 45 minutes with 2Θ range 24°-33°. Then the semi-quantification of the carbonates was obtained by normalizing the areas of the diffraction peaks of identified minerals (aragonite 3.39 Å; calcite 3.03 Å; dolomite 2.88 Å) with respect to the percentage of areas coming from an equi-mass mixture of carbonates, then setting the ratio of the normalized area of each carbonate to the sum of the standardized areas. Associated to the relative percentages of these carbonates, carbonate crystallinity was measured on the main peak through full width half maximum (FWHM). This index determined by measuring the enlargement of the carbonate peak likely reflects the authigeny of the crystal. Indeed, according to Fontes et al. (1993, 1996), detrital, well crystallized carbonates display thin shape of the peak and thus low values of crystallinity index while for authigenic carbonates that are less well crystallized, this index is high (Fontes *et al.*, 1993; Fontes *et al.*, 1996).

3.2.3. Radiocarbon chronology

The ^{14}C time-scale has been defined through 13 AMS dating both on (i) organic fractions including diffused organic matter and hand-picked charcoal, and (ii) carbonates fractions on inorganic fractions and on hand-picked shrimp's fecal pellets when existing.

Each organic fraction was submitted to the standard chemical protocol for AMS analyses: 3 successive hydrochloric acid/sodium hydroxide/hydrochloric acid baths, followed by several rinses with deionized water up to neutral pH, and gently drying-up at 60 °C overnight.

The CO_2 gas was obtained (i) for organic samples by burning at 860 °C for 30 min, under vacuum, in presence of a mixing of copper(II)-oxide/copper(III)-oxide and silver thread, and (ii) for carbonates, by an H_3PO_4 acid attack under vacuum during one night in a thermostatic bath. Then, AMS-^{14} C targets were obtained by graphitization of the CO_2 gas on powdered iron with hydrogen at 650 °C for 100 min, and graphite compression under analytical plots. Aliquot of the CO_2 gas was then used for associated ^{13}C measurement. Graphite sources were prepared in GEOPS laboratory, and counted by the accelerator mass spectrometer at LSCE laboratory (ECHoMICADAS facility, France).

Analytical uncertainties, including laboratory errors, are ± 0.1‰ for δ ^{13}C and between 0.5 and 0.8 pMC for ^{14}C activity. All the dates are converted to calendar ages according to the revised calibration program CALIB 8.2 (Execute Version 8.2 html 2020; Table 2) (Reimer *et al.*, 2013; Reimer *et al.*, 2020; Stuiver *et al.*, 2021).

4. Results

4.1. Catchment area samples

The results of grain size, bulk sediment mineralogy and clay minerals analyses of 8 samples from the main geological formations are presented in Table 3. Grain size distribution indicates that the silt fraction predominates in all samples, ranging from 67.5 to 85.2%. In the silty fraction, coarse silt with 36.3 to 53.9% presents higher content than the fine one with 15.7 to 38.4% respectively; only sample 6 shows both two

fractions in the same proportions. The second dominant fraction is sand ranging from 9.3 to 28.3%, while the clayish fraction remains at low contents, i.e. between 2.2 and 5.8%.

Considering bulk sediment samples, several groups of minerals are identified such as (i) carbonates (calcite and dolomite), (ii) silicates: quartz, mica (muscovite), feldspar (albite, orthoclase, anorthite), amphibole (hornblende), clays (chlorite, kaolinite, illite, smectite and some palygorskite), and (iii) oxides and hydroxides: rutile, magnetite and goethite. Among these minerals, the most frequent ones have been semi-quantified (Table 3).

As a whole, calcite and quartz are predominant. Quartz varies between 7.3 and 55.8% and reaches the highest values (31.7 and 55.8%) in samples 2, 6 and 7. Calcite prevails in samples 1, 3, 4, 5 and 8, ranging from 53.9 to 79.3%, while it is absent in sample 6. Dolomite is only present in samples 1, 2, 3, 5 and 8, and varies between 5.8 and 18.5%. Low values of crystallinity index obtained for calcite and dolomite in all units where they occur (0.08-0.12) indicate that they are well crystallized (Fontes *et al.*, 1993; Fontes *et al.*, 1996).

In all samples, clays, mica and feldspars are in relatively low contents except sample 6, in which the high values are 19.1%, 29.8% and 19.3%, respectively. Further analysis of the clay assemblages in the clay-sized siliceous fraction, which allows more accurate estimates than in the bulk sediment, shows that smectite and illite are the most common (Table 3). Smectite is predominant in samples 1 and 7, with 58.2 and 72.7%, respectively. Meanwhile, the ratios of smectite/illite (S/I) in these two samples are more than 3. Illite prevails in samples 3,5,6 and 8, ranging from 42.4 to 52.0%, as a consequence of the S/I ratio much smaller than 1. In samples 2 and 4, smectite and illite display similar percentages with a S/I ratio about 1. Kaolinite and chlorite reach lower values as a whole. Chlorite shows the same change pattern with illite and one can observe that chlorite contents are quite high reaching even to 31.9% in samples where illite dominates. Nevertheless, it is very low in sample 7. Kaolinite remains at about 10%, with however higher values for samples 5 and 8 (ca 18%) and lowest value for sample 7 (2.2%).

The illite chemistry index of all eight samples is less than 0.4 (Table 3), suggesting Fe- and Mg-rich illites as it was proposed by Diekmann et al. (1996) and Ehrmann et al. (2005). In addition, smectite and illite crystallinities of these samples are ranging from 0.27 to 0.76 and from 0.17 to 0.30 respectively. Being less than 1.50 for smectite and less than 0.40 for illite, these values indicate well-crystallized clay minerals (Diekmann *et al.*, 1996; Ehrmann *et al.*, 2005).

4.2. Lake sediments

4.2.1. Lithology

The 8-m long Golman 6 core presents two major sedimentary sequences, under and upper the 4.52 m depth (Fig. 2a). In the lower part from 8.00 to 4.52 m depth, quite fine, grey silty and clayish sediments dominate while the above 4.52-4.23 m interval is composed of sandy and silty deposits. In the last section of the upper part in Golman 6 core has been compacted to the 4-3.15 m interval from 4-0 m during coring. The Golman 7 sequence is 12.5 m long and also divided into two major sequences separated by an empty interval due to missing sediment between 8.65-4.20 m (Fig. 2b). The lower part between 12.50 and 8.65 m depth is mainly composed of grey silts and clays while the above section from 4.20 m to the core top at 1.60 m depth encloses several lithological variations highlighted, similarly as in the Golman 6 core, by changes in the grain size, color and nature of the sediment.

The lacustrine sedimentation depicted in these two cores evidences the same lithological succession, although with slight differences in unit thicknesses. In order to better integrate and therefore interpret all the results as a whole set of data, a single stratigraphic sequence was reconstructed based on lithological changes as well as on carbonate contents and magnetic susceptibility (Tudryn *et al.*, 2021). The composite sequence defined thus displays the complete Lake Urmia sedimentation from 12.50 m depth to the core top at 1.60 m depth with the following major lithological units (Fig. 2c).

The lower unit 1 between 12.50 and 4.52 m depth begins with sub-unit 1a, from the core base to 12.38 m depth, consisting in brownish sand followed by a dark grey, organic-rich black event at 12.48-12.43 m interval and then by grey silt above. From 12.38 to 4.52 m, the sub-unit 1b consists of grey silty/clayish deposits (Fig. 2d) containing some 1-mm thick sandy levels interbedded and an interval between 8.87-8.65 m marked by higher contents of silt and sand. Unit 2 presents a much more heterogeneous pattern with successive sub-sections as follows: (i) sub-unit 2a between 4.52 and 4.02 m depth consisting in brown sand and silt (Fig. 2e); (ii) sub-unit 2b from 4.02 to 3.85 m, made of homogeneous grey silts and clays; (iii) sub-unit 2c comprised between 3.85 and 3.73 m, containing grey and dark grey sand; (iv) sub-unit 2d at 3.73–2.87 m depth and formed by homogeneous grey clayish levels; (v) sub-unit 2e made of sandy and silty layers from 2.87 to 2.20 m depth (Fig. 2f), overlaying a 8-cm dark grey and black organic rich level, and (vi) sub-unit 2f that consists in grey sand from 2.20 to the core top at 1.60 m depth.

In addition, the two sub-units 2d and 2f contain lots of fecal pellets from the development of the brine shrimp *Artemia urmiana* in the lake (Fig. 2g-i). These pellets are white, sometimes dark, and they constitute almost 90% of many levels of sub-unit 2d (Fig. 2h). In the lower unit 1, fecal pellets are absent except for only few thin levels, in which some white pellets have been observed at 9.86 m and 10.92 m depth. These 50–200 μm, white fecal capsules of brine shrimp *Artemia* are considered as authigenic sedimentary component, although composed of a mixture of carbonates with minor amounts of siliclastic particles (Kelts and Shahrabi, 1986; Sharifi *et al.*, 2018). According to Kelts and Shahrabi (1986), fecal pellets are composed of more than 80% aragonite in modern sediment beds, while when they are darker in color, it is suggested that fecal pellets are older reworked. According to the studies in Great Salt Lake, the presence of fecal pellets in the sediment indicates that *Artemia* thrives in the water salinity between 100 and 300 $g.L^{-1}$ but its tolerance of salinities can extend up to about 340 $g.L^{-1}$ (Post and Youssef, 1977; Sharifi *et al.*, 2018). For a water salinity lower than 100 $g.L^{-1}$, the decrease in the shrimps population is explained by increasing predators, while in a water salinity more than 300 $g.L^{-1}$, *Artemia* can hardly live (Wurtsbaugh and Gliwicz,

2001; Agh *et al.*, 2008; Esmaeili Dahesht *et al.*, 2010). In addition, when the lake water temperature is less than ca 3 °C, the shrimps are completely absent (Wurtsbaugh and Gliwicz, 2001).

4.2.2. Grain-size distribution

The distribution patterns of major grain-size classes for the siliclastic fraction of Lake Urmia sediments are shown in Fig. 3. The results reveal that silt is the dominant size fraction throughout the sequence as the whole, ranging from 33.3% to 93.1%. The lower sequence in the 12.38-4.52 m interval, presents higher contents and a more stable composition of clays and silts than that of the upper sequence (4.52-1.60 m), which is marked by a saw tooth increase in sand content and by a low clay fraction however broadly correlated to the silt content.

The core base between 12.50 and 12.38 m depth (sub-unit 1a), is characterized by the predominance of sandy and coarse silty fractions. The following section between 12.38-4.52 m (sub-unit 1b), presents a broadly stable grain size distribution with 49.8% of fine silt, 31.5% of coarse silt, 12.5% of clay and 6.2% of sand. Nevertheless, at the top of this section (6.00-4.52 m), the clayish fraction increases while coarse silt decreases. The whole sequence exhibits low and unvaried values of mode, median and mean.

Between 4.52 and 1.60 m, grain size displays sharp changes, quite well correlated with the identified lithological unit 2 and as a whole, with increasing coarse silt and sandy fractions when compared with the lower unit 1. The clayish fraction is low and follows the fine silt pattern that reaches its highest content in sub-unit 2d and relative high content in sub-unit 2b. The most important variations are pointed out by the sandy and fine silty fractions varying between 4.52 and 4.02 m and between 3.85 and 3.73 m in levels 2a and 2c, respectively. These two grain sizes, as well as mode and median highlight the bi-modal sub-unit 2e with increased sandy fraction in its lower part and increased fine silts in its upper part. In combination with mode, the most frequently-occurring particle diameter, as well as median, corresponding to the 50 percentile on a cumulative curve, the mode/median ratio could indicate the predominate particles as fine,

coarse, or equal contents of both. As presented in Fig. 3, the mode/median ratio at 12.38-4.52 m and 3.73-2.87 m intervals is less than 1, reflecting the dominant fine fraction while other depths are characterized by coarse fraction.

Finally, the different proportions of clay, silt and sand in lake sediments and in the catchment area, reflect the sorting of the detrital material during the river transport and depositional conditions.

4.2.3. Mineralogy

In combination with Fig. 4 and Fig. 5, XRD analyses on samples from the composite core indicate the present of (i) silicates dominated by quartz, feldspars (orthoclase, albite), mica (muscovite) and clay minerals (chlorite, illite, kaolinite, smectite and some palygorskite), all identified in the whole set of samples, and in some specific levels, minerals from amphibole and pyroxene groups as well as iron oxides (magnetite) that are of detrital origin; (ii) carbonates that can be detrital, biomediated or chemically precipitated whether in evaporitic environments or not; (iii) evaporitic minerals as halite and gypsum, and (iv) other minerals such as iron sulfides (greigite and pyrite) that are of early diagenetic origin.

The presence of evaporitic minerals, such as halite and gypsum in almost all the samples, points out relatively saline to highly saline conditions in the lake during all concerned period (Fig. 4d).

4.2.3.1. Quartz, feldspars and mica

Quartz, as well as feldspars and mica display the same pattern with increased contents at the core bottom (sub-unit 1a), and in three above sections of the unit 2 (sub-units 2a, c and e), with 38%, 27% and 28% of the total sediment respectively (Fig. 4). The lowest contents of these minerals, even less than 1%, are recorded in sub-unit 2d. According to the results obtained from the catchment area, the geological formation 6 and possibly some others (formations 2, 7) represent important sources for these three minerals. When these minerals are in lower contents, their origin cannot be clearly identified, but one can observe that the

lowest contents of this mineralogical assemblage as in the sub-unit 2d, are in the geological formations 4, 5 and 8.

4.2.3.2. Clay minerals

Among all clay minerals in the clay-sized siliceous fraction, illite and smectite dominate the lake sedimentation (Fig. 5), less abundant chlorite fluctuates similarly to illite, kaolinite shows lowest percentages. Sediments from unit 1 (12.50-4.52 m), are characterized by relatively stable proportions of different clay minerals with the predominance of smectite (51.9%), followed by illite (33.2%), chlorite (11%) and kaolinite (4.3%). The upper unit 2 demonstrates more contrasted clay minerals pattern. Sediments in the 4.52-3.73 m interval that correspond to sub-units 2a, 2b and 2c, exhibit (i) increasing proportions of illite (up to 62.0%) and chlorite, (ii) decreasing contents of smectite (until 10.3%), and (iii) low and stable proportions of kaolinite. In sediments comprised between 3.73 and 2.87 m, i.e. sub-unit 2d, both smectite and illite present relatively stable and equal proportions of 40%. The two last units 2e and 2f units exhibit broadly the same pattern with relatively low, changing contents of smectite (13.7%) and high, fluctuating contents of illite (61.3%). Chlorite reaches its highest values of 26.2% in sub-unit 2e before decreasing while kaolinite stays low overall the whole core and just increases up to 18.4% at the top sequence. The composition variations of different minerals throughout the whole composite core reflect quite a good agreement with different lithological formations from the catchment area. Indeed, high contents of smectite in the lake sediment are also recorded in the catchment area for geological formations represented by samples 1, 2, 4 and 7. Illite rich sediments that display increased contents of chlorite too, are present in samples 3 and 6, but also in 2, 5 and 8. Finally, the high contents of kaolinite in the upper part of the core are also recorded in samples 5 and 8.

Smectite crystallinity index is around 0.8 in the lower part of the core (unit 1) and scales further above but still remaining below 1.5. Meanwhile illite crystallinity in the under lying unit 1, varying values between

0.2 and 0.5 that reflect very well- to well- crystallized illite, suggests some chemical transformations (Ehrmann *et al.*, 2005). As values obtained for samples from the catchment area (Fig. 5), they indicate well crystallized smectite and illite (Ehrmann *et al.*, 2005). In the upper sequence named as unit 2, illite crystallinity index remains stable and low, equaling to 0.1-0.2 that indicates very well crystallized illite, which is well correlated with samples in the catchment area. Illite chemistry index fluctuates around 0.2 all throughout the sediments. This parameter when lower than 0.4, reflects Fe and Mg-rich illite (Diekmann *et al.*, 1996; Ehrmann *et al.*, 2005). The illite chemistry as well as illite and smectite crystallinities in the core sediments present values identical to those of the formations of the catchment area, thus suggesting the high stability and detrital origin of the clays, acting rather by erosion than chemical weathering.

4.2.3.3. Carbonates

Carbonate contents display values from ca 20 to 93% and their variations are correlated with defined lithological units (Fig. 4e). Unit 1 starts with low values of about 20% that increase at the beginning of sub-unit 2b up to 60% and remain relatively stable throughout the core. Above unit 1, carbonate contents clearly fluctuate: they decrease to 20-25% in sub-units 2a, 2c, 2e and increase in 2b, 2d and 2f reaching the highest values of 93% in sub-unit 2d. The carbonate curve evidences the same succession of environmental changes to that obtained by Tudryn et al. (2021), although due to different method used, either the calculations from XRD diagrams applied in the present study or the Mélières mono-calcimeter (Tudryn *et al.*, 2021), the values are different. The former might be slightly overestimated due to a fraction of non-crystalline material that may be present in the sample, while the latter allows calcium carbonate to be measured but not the most resistant dolomite.

Carbonate fraction consists of three minerals: calcite, aragonite and dolomite (Fig. 4). Aragonite is absent in sub-units 1a, 2a, 2c and 2e, whereas it is present elsewhere in the sediment either as mud or as major component of fecal pellets. Aragonite represents the major part of the carbonate fraction with percentages

even as high as 92% where shrimp's fecal pellets are particularly abundant (sub-unit 2d, Fig. 2h) and its general pattern is similar to that of total carbonate. Calcite and dolomite evolve as a whole between 0 and 15%. In the very narrow sub-unit 2b calcite reaches the highest content of 38% and then contains low and stable content from sub-unit 2d to the core top, it displays inversed pattern to that of aragonite. Dolomite also displays such inversed pattern to aragonite all along the sequence with clear increases of percentages in sub-units 1a, 2a, 2c and 2e (Fig. 4).

The calcite crystallinity index presents values of about 0.10 along the core. A single level is characterized by the highest calcite crystallinity index of 0.26 shown in sub-unit 2b (Fig. 4). Since (i) the higher value the crystallinity index, the worse the carbonate is crystallized, and (ii) calcite crystallinity obtained for samples from the catchment area ranges between 0.08 and 0.12, it appears that most of the calcite in the core sediments present the same good crystallinity and is thus of detrital origin. According to Fontes et al. (1993, 1996), only the calcite found at depths from the sub-unit 2b can be considered as authigenic rapidly precipitated through biogenic activity or through direct chemical precipitation in lake water.

The crystallinity index of dolomite in lake sediments displays scattered values between 0.06 and 0.38 while it is evolving from 0.08 to 0.12 in samples from the catchment area. Following the example of calcite, well-crystallized dolomite is thus of detrital origin (low index value; sub-units 1a, 2a, 2c and 2e), while its poor crystallinity is related to authigenic conditions of precipitation (high index value; sub-units 1b, 2b, 2d and 2f). The formation of dolomite requires drastic chemical conditions rarely found in lacustrine environments except when occurring as in situ replacement product of calcium carbonate sediments, particularly in evaporitic sites (Pierre *et al.*, 1984). However, dolomite precipitation is driven by both high alkalinities and low Ca^{2+}/Mg^{2+} and SO_4^{2-} concentrations in the solution, the two latter resulting of massive calcium minerals precipitation (carbonates, sulfates) and/or a bacterial sulfate reduction (Lippmann, 1973). In Lake Urmia composite core, the direct crystallization of dolomite from aqueous solutions could be considered in relation with highly evaporative phases (alkaline status of the lake) as observed in the Coorong area in Australia or

in the Deep Spring Lake basin in California (Alderman and Skinner, 1957; Alderman and Von Der Borch, 1960; Alderman and Von der Borch, 1961; Alderman and Von der Borch, 1963; Peterson *et al.*, 1963; Skinner, 1963; von Der Borch, 1965; Peterson and Bien, 1966; Clayton and Jones, 1968; Von der Borch and Jones, 1976). Moreover, dolomite precipitation occurs concomitantly with the formation of aragonite that (i) displays high crystallinity index (Fig. 4k), (ii) requires a high Mg^{2+} content in waters to become the stable species of calcium carbonate and (iii) can be related to the chemical or biochemical precipitation, both reflecting evaporative conditions (Müller *et al.*, 1972; Eugster *et al.*, 1983; Kelts and Shahrabi, 1986; Fontes *et al.*, 1993; Fontes *et al.*, 1996).

4.2.4. Chronology

The ^{14}C AMS dating performed both on organic fractions (diffused organic matter and hand-picked charcoal) and on inorganic and biomediated (i.e. fecal pellets) carbonates from cores Golman 6 and Golman 7 are presented in Table 2.

Considering all the data gathered on the carbonate fraction over the composite core and on the catchment as well as the modern hydrogeochemical lake system, we have to implement two age corrections: (i) the first one related to the detrital carbonate fraction in the dated samples, and (ii) the second one taking into account the hard-water effect of the modern lake surface water, considering that authigenic materials such as inorganic carbonates and organic matter are formed in the lake upper water layer.

(i) Correction 1 is applied on bulk samples when a detrital carbonate fraction is evidenced; the ^{14}C activity of the authigenic carbonates can be written as $A_M = X*A_{AC} + A_{DC}*(1- X)$ with A_M, the measured ^{14}C activity on the total carbonate fraction; X, the percentage of authigenic carbonate in the bulk sample; A_{AC} and A_{DC}, the ^{14}C activities of the authigenic and detrital carbonates respectively. Assuming that detrital carbonate originating from the watershed is ^{14}C-free ($A_{DC} = 0$), we can state $A_{AC} = A_M /X$ as proposed by Fontes et al. (Fontes *et al.*, 1993; Fontes *et al.*, 1996). This correction is applied on all the dated samples

containing a detrital fraction, either calcite or calcite and dolomite through XRD half-width of the main peak for each mineral (Table 2): both of dolomite and calcite are considered as detrital (authigenic) when their crystallinity indexes are lower (higher) than 0.12 according to the crystallinity index of catchment samples.

(ii) Correlation 2 is applied on ^{14}C dates established from carbonate activities after correction 1 if a detrital fraction is present in the bulk sample; knowing that the ^{14}C activity of atmosphere CO_2 was measured at 101.8 pMC in 2016 (Hua *et al.*, 2021), the present-day ^{14}C activity of the lake water is 680 yr. The most common hypothesis is to consider that this reservoir effect in the past (Fontes *et al.*, 1993; Fontes *et al.*, 1996; Gasse, 2000). However, when ^{14}C dates are plotted against depth, a consistent evolution appears with all carbonate and organic levels dated above 6 m depth (above 22 kry BP). With respect to the ages defined on charcoal which represent the equilibrium with atmospheric CO_2, a different of 2000 years can be defined which can be applied to all the other ages.

From 12.5 to 4.52 m depth, the ^{14}C AMS chronology is based on 4 dating that are in agreement with the lithostratigraphy, with a sedimentary rate (msr) of 0.89 mm.yr-1 (Table 2). This msr is relatively high due to the presence of unrecovered muddy sections during coring, which artificially increase the sedimentation rate. From 4.52 m depth to the core top, two phases are recorded, i.e. 4.52-2.87 m and 2.87-1.6 m intervals, associated to msr of 0.12 and 0.40 $mm.yr^{-1}$ respectively.

5. Discussion

5.1. The palaeoenvironmental history of Lake Urmia

Lake Urmia is a complex hydrological system governed by the climatic evolution in the eastern Mediterranean area and Western Asia, but also by local factors. Among local factors, the topography,

geology and tectonics in the catchment area as well as the lake basin hydrology, which is driven by the net effect of precipitation, surface runoff, evaporation, and evapotranspiration processes (Eugster and Jones, 1979), are of upmost significance during depositional processes in the lake. In its south western part of Lake Urmia concerned by this study, the contrasting topography and differences in altitude of more than 1500 m between the most distant sources of detrital material and the lake favor erosional processes independently of the climate and water availability. Magmatic, metamorphic and sedimentary rocks are present in the catchment and minerals from these rocks constitute an important part of the lake sediments. Carbonates, feldspars and mica undergo chemical alteration relatively easily among all these minerals (Chamley, 1989). These detrital minerals are dramatically poor in two sub-units of the unit 2 (2b: 4.02-3.85 m; 2d: 3.73-2.87 m), while elsewhere they represent a major part of the sediments and highlight rather erosional processes in the catchment area than chemical ones. Additionally, the authigenic carbonate integrating the aragonite fraction either chemically or biological mediation precipitated, represents a significant part of the lake sediments. Halite and gypsum indicate the evaporitic conditions in the lake basin as a whole. Iron sulfides identified in several parts of the sediment highlight the early diagenesis in the sediment in anoxic, sulfate-reducing environment (Tudryn *et al.*, 2021). Despite the complexity of ^{14}C signatures of authigenic carbonate and from organic matter samples (either terrestrial or lacustrine) we established a reliable chronology of the lake evolution for the last 30 kyr. As the age scale of composite core is presented in Fig. 6, the data reflect the lake history both general climate trends and fundamental changes in local hydrology through well-defined intervals.

5.1.1. The lake at ca 30 cal kyr BP

The interval starts with light brown sandy sediments and is followed by coarse silt of blackish to dark grey color due to abundant vegetation remains. This sequence is characterized by high contents of detrital silicates, including both predominant coarse particles (such as quartz, feldspars and mica) and few fine

particles (Fig. 6). In addition, a low abundance of aragonite-free carbonates is recorded with the presence of calcite and dolomite, both from detrital origin. Such a sedimentary composition dominated by coarse grain sizes indicates the direct influence of the Shahr Chay River at the coring site and erosional processes in the catchment rather than chemical weathering that implies water availability. Silicates originating principally from phyllite and sandstone, are present in the upper part of the catchment area (geological formation sample 6 in Table 3), while calcite and dolomite derive from carbonate rich formations 3 and 8. According to Tudryn et al. (2021), the light brown sand at the beginning of the interval and the presence of detrital magnetite highlight well oxygenated conditions during the sedimentation at the coring site. Moreover, pressurized gas and brine are captured in this sand with less water salinity than in today's lake waters. Above the sandy level, blackish and dark grey silts are rich in plant remains identified as C_3 plants with $\delta^{13}C$ around -25‰ PDB (Table 2) and in greigite, an authigenic iron sulfide that indicates the anoxic and sulfate-reducing conditions within the sediment (Curtis, 1987). Greigite being magnetic mineral, its presence is highlighted by high magnetic susceptibility on Fig. 6a. As noted by Tudryn et al. (2021), the high organic content here may reflect an increased input of organic detritus from the river, although the decreasing grain size of the sediment and its poor oxygenation more likely suggest the development of a saltmarsh with high biological productivity rather than a higher riverine activity.

Such a start of the sedimentary sequence reflects erosional processes in the catchment and a low lake level, without lacustrine or very shallow conditions in the coring area, reflecting rather dry conditions and a low water availability on the catchment area.

5.1.2. The 29.85-20.21 cal kyr BP interval

The grey, homogeneous sedimentation is dominated by fine silts and clays, with some interbedded millimetric levels of coarse silt and sand. Detrital silicates (mainly quartz, mica and feldspars) represent about 30% of the sediment. In the clay fraction, well-crystallized smectite dominates reaching the highest

contents of the whole sequence (12% in total sediment). The ratio smectite *versus* illite stays close to 2, indicating broadly invariable proportions of these minerals all along the interval (Fig. 6). This is compatible with the erosion of the geological formations 7 and 1, as well as 4 and 2, that bring abundant smectite from the catchment area enough to explain the high smectite contents. However, chemical ongoing weathering or precipitation in the lake salty environment (Chamley, 1989) cannot be totally excluded since (i) halite is present here (but also all along the core), and (ii) smectite related to the chemical weathering especially in the formations 7 and 1, would indicate enough water in the catchment for such process. In addition, carbonates account for 62% in the suite of minerals with 38% of aragonite, 16% of calcite, and 8% of dolomite, in which aragonite is of authigenic origin and calcite is of detrital one, while dolomite has both authigenic and detrital origins according to their respective crystallinity indexes.

Such detrital fraction in the core sediment suggests that the environment is still dominated by physical weathering and erosion on the catchment area, with nevertheless, low transport energy conditions, reflecting lacustrine conditions established in the coring site. At the beginning of the interval, aragonite that was absent before at the core base appears and increases rapidly from 25 to 50% of the sediment, while authigenic dolomite occurs in several parts of the interval, both constituting the carbonaceous mud. The formation of both aragonite and dolomite requires a high Mg^{2+} content in waters to become the stable species of calcium and magnesium carbonates, and thus reflect evaporative lacustrine conditions (Alderman and Skinner, 1957; Alderman and Von Der Borch, 1960; Alderman and Von der Borch, 1961; Alderman and Von der Borch, 1963; Peterson *et al.*, 1963; Skinner, 1963; Peterson and Bien, 1966; Clayton and Jones, 1968; Müller *et al.*, 1972; Eugster *et al.*, 1983; Kelts and Shahrabi, 1986), as do halite and gypsum. The intensity of evaporative conditions probably experienced several fluctuations that can be deduced from the decrease of evaporate minerals and the simultaneously decrease of authigenic dolomite between 26.50 and 24.30 kyr BP, and at ca 22.90 kyr BP (Fig. 6g and i).

Detrital and authigenic fractions of the sediment show a clearly lacustrine environment established at the coring site during this interval. Meanwhile, the quite small grain size suggests low transport energy conditions in phase with a relatively high water level. The water salinity fluctuation is highlighted by simultaneous changes in the authigenic dolomite contents and evaporites. The interval is characterized by relatively wet although cold conditions that favor erosional processes in the catchment area even if chemical weathering was probably acting too.

In addition, according to previous studies (Wurtsbaugh and Gliwicz, 2001; Abbaspour and Nazaridoust, 2007; Agh *et al.*, 2008; Esmaeili Dahesht *et al.*, 2010), the absence of fecal pellets could be attributed to (i) very low lake level and thus too highly saline conditions for shrimps development (more than 300 $g.L^{-1}$), or (ii) a very high water level with too low salinity (below 100 $g.L^{-1}$) implying the presence of predators that do not allow the shrimps development, or (iii) very cold lake water that also do not allow the shrimps development (ca 3 °C). However, this sequence (apart two thin levels) could reflect a very high water level with cold temperature.

Finally, Tudryn et al. (2021) showed that magnetic minerals point out early diagenetic processes in anoxic sediment and possibly a bad ventilation of the bottom water, in good agreement with a high lake level. Additionally, the decrease of illite crystallinity within this time interval could also be related to the specific post-deposition environment in the lake sediments. The data thus indicate that after a low lake stand at ~30 cal kyr BP, the lake level increased and, nevertheless some fluctuations, remained high until 20.21 cal kyr BP.

5.1.3. The 20.21-15.33 cal kyr BP phase

Sediments of the 20.21-15.33 kyr BP interval consist in (i) brown sands and silts with high contents of silicates as quartz, mica and feldspars, quick and short time illite and chlorite peaks, decrease of smectite and (ii) low carbonate contents with no aragonite, some calcite and more dolomite, both of detrital origin

as indicated by their low crystallinities. These parameters thus indicate detrital input into the core site associated to physical weathering with erosion from geological formation 6 and dolomite-rich formations 3 and/or 8, and with no authigenic minerals. It is suggested that sediments during this period were deposited in relatively dry conditions, a low lake level and a well-oxygenated environment.

5.1.4. The 15.33-13.27 cal kyr BP interval

This following sequence is characterized by increasing clays and fine silt, in which silicates as quartz, mica and feldspars, only account for 20% (Fig. 6). With 66.2% of total sediment, the carbonate mud is made of aragonite (31.6%), calcite (23.5%) and dolomite (11.1%). According to the crystallinity index values, both dolomite and calcite are entirely of authigenic origin. Meanwhile these parameters clearly indicate lacustrine conditions as the same with 29.85-20.21 cal kyr BP interval. In contrast, the presence of the authigenic calcite between 15.33 and 13.27 cal kyr BP suggests less evaporative conditions than before, without authigenic calcite (Müller *et al.*, 1972). Even if slightly advanced, two thousand years lasting in this interval shows timing in good agreement with the Bölling/Alleröd warming within Post-Glacial period as observed through Greenland ice cores (Fig. 6j).

5.1.5. The 13.27-11.82 cal kyr BP interval

The environmental conditions are similar to those recorded between 20.21 and 15.33 cal kyr BP. Indeed, sediments are marked by an increase in grain sizes and detrital silicates input, the dominance of illite and chlorite in the clayish fraction and the decrease in carbonate contents. Within carbonate fraction, aragonite is absent while few calcite and abundant dolomite of detrital inputs are present. All these parameters as well as the presence of magnetite indicate a well-oxygenated and close to the river mouth environment at the coring site, indicating a very low lake level. This regressive stage of the lake corresponds to the Younger Dryas cooling before the Holocene (Fig. 6j).

5.1.6. The 11.82-5.64 cal kyr BP interval

The sequence is characterized by fine-grained sediments, with very low contents of detrital minerals and the predominance of an authigenic carbonate fraction, indicating clearly the re-establishment of open lacustrine conditions. The detrital fraction of this section has higher clay mineral contents than the underlying section, and contains equal proportions of smectite and illite, with some added detrital calcite. In the carbonate fraction, authigenic dolomite and huge contents of aragonite are present in the calcareous mud, mainly under the form of aragonite shrimp fecal pellets that are the dominant component of the sediment (Fig. 2 and 7). The presence of these minerals indicates a lacustrine environment with high water salinity as like the period recorded at 29.85-20.21 cal kyr BP during which nevertheless, the presence of the shrimps *Artemia* is not recorded. According to previous studies, the abundance of *Artemia* fecal pellets is related to the water salinity between 100 and 300 $g.L^{-1}$ and other parameters including temperature, that make favorable conditions for shrimps development (Wurtsbaugh and Gliwicz, 2001; Agh *et al.*, 2008; Esmaeili Dahesht *et al.*, 2010; Sharifi *et al.*, 2018). In several levels, dark and white pellets are mixed, the dark ones being older and reworked according to Kelts and Sharabi (1986). The presence of some iron sulfides, suggests a bad ventilation of the bottom water (Tudryn et al., 2021). The end of this section is marked by sharp changes in the lithology and all parameters (Fig. 2c and 7).

5.1.7. The 5.64-4.10 cal kyr BP spell

This interval is divided into two parts. The lower part is characterized by coarse, sandy black sediment with abundant organic remains and authigenic iron sulfide, *i.e.* greigite. The ^{14}C dating performed on charcoal at 2.80 m depth gives an age of 5.48 cal kyr BP, in good agreement with the 4.94 cal kyr BP age also obtained on charcoal and collected from the neighboring core Golman 5 at 2.66 m depth indicated by Tudryn et al. (2021). In the upper part of this sequence, silty and detrital minerals prevail, mainly with

quartz, feldspar, mica, illite, and few carbonate-calcite and dolomite being of detrital origin too. This suggests the drying out or very shallow conditions at the coring site similarly to what is recorded at the beginning of the sequence *i.e.* at ~30 cal kyr BP. Nevertheless, contrary to the core bottom, the dated charcoal samples exhibit distinct $\delta^{13}C$ values of -26.5, -25.5 ‰ and of -13.5, -14.5 ‰ vs PDB (Table 2), characterizing C_3 and C_4 plants respectively and emphasizing that both coexist on the watershed at the time of deposition. The C_4 vegetation episode seems to have lasted at least 600 years, between 5.64 and 4.10 cal kyr BP, and likely indicates a warmer and drier episode than the one occurring at 30 cal kyr BP.

5.1.8. The 4.10 -2.34 cal kyr BP interval

Abundant shrimp fecal pellets are found in this last sequence, reflecting the lake level rise and thus a recover of open lacustrine environment at the coring site. The predominant sandy fraction made of detrital silicates reflects a high energy transport from the nearest inflow, Shahr Chay River. Furthermore, the high carbonate content gathers authigenic aragonite and dolomite as well as some detrital calcite. Authigenic carbonates and shrimp fecal pellets indicate a high evaporation rate, with a water salinity comprised between 100 and 300 $g.L^{-1}$, and temperature high enough to allow the shrimp development (Sharifi *et al.*, 2018).

5.2. Lake Urmia history at a regional scale

The results obtained here show the importance of detrital input related to the physical weathering in the catchment area and indicate several Lake Urmia low and high stands. The intense erosional processes have also been described by Mirzapour et al. (2021a; 2021b). The lake water level changes clearly mark the alternation of relatively dry and wetter periods in the lake catchment, but still with high evaporation conditions and saline lake waters even in the wettest periods.

After the low stand at ~30 cal kyr BP, the lake level increased and remained high until the Last Glacial Maximum at ca 20 cal kyr BP at the coring site. Our results confirm those obtained by Djamali et al. (2008a) who proposed a high water level during the last glacial period, on the opposite to Stevens et al. (2012) that indicated no perennial lake and clearly arid climate at Lake Urmia. Moreover, our results are in good agreement with evolution of surrounding lakes at a regional scale such as the high stands reported from Lake Zeribar (Wasylikowa *et al.*, 2006) and Lake Van (Kuzucuoğlu *et al.*, 2010) as well as from the Black Sea (Shumilovskikh *et al.*, 2014).

From 20.21 to 2.34 cal kyr BP, the lake experienced water level fluctuations with three relatively high stands (i) between 15.33-13.27 cal kyr BP during the warming Bolling/Alleröd event, (ii) from 11.82 to 5.64 cal kyr BP, during the Early and Mid-Holocene and (iii) during the 4.10-2.34 cal kyr BP, Late Holocene interval registered in our cores. These intervals were separated by low lake stands with completely dried-out or close to the lake water line conditions at a coring site (i) after the Last Glacial Maximum between 20.21 and 15.33 cal kyr BP, (ii) during the Younger Dryas from 13.27 to 11.82 cal kyr BP, and (iii) at the transition from Mid to Late Holocene, during the 5.64-4.10 cal kyr BP interval (Fig. 6). Previous studies by Kelts and Shahrabi (1986) on Lake Urmia identified 3 relatively high lacustrine stands and 2 low ones for the Late Pleistocene and Holocene, and proposed ca 9-7.5 kyr BP for the lacustrine period that certainly corresponds to that between 11.82-5.64 cal kyr BP in our record; indeed, authors highlighted the lack of readily dateable material in their study. Stevens et al. (2012) indicated dry conditions with the short-term lacustrine episode at ~14 kyr, drying out probably marking the Younger Dryas and no re-establishment of lacustrine conditions until ca 10 kyr. Holocene reconstructions by Sharifi (2018) suggested wet early Holocene and frequent dry episodes during Mid-Late Holocene.

The lacustrine records from Zagros Mountains (lakes Zeribar, Mirabad, Dasht-e Arjan) indicate dry conditions and low lake levels during the early Holocene (Stevens *et al.*, 2006; Wasylikowa *et al.*, 2006; Aubert *et al.*, 2019), while clearly lacustrine conditions dominated in Lake Urmia during this time. Quite

wet conditions at the beginning of the Holocene, and changing ones during the Late Holocene, are also indicated from Lake's Neor basin area located in the NW Iran (Sharifi *et al.*, 2015; Aubert *et al.*, 2017), and from Anatolian lakes (e.g. Van, Gölhisar, Eski Acigöl). According to many authors, Anatolian lakes were subject to evaporation during the Mid-to-Late Holocene, when water levels fell and even led to the lake drying out (Landmann *et al.*, 1996; Roberts *et al.*, 2001; Eastwood *et al.*, 2007; Jones *et al.*, 2007; Jones and Roberts, 2008; Roberts *et al.*, 2008).

In Lake Urmia, transition from Mid to Late Holocene was marked by dry conditions and a low water level between 5.64 and 4.10 cal kyr BP. Such a dry event was identified during broadly the same time in Zagros Mountains (Stevens *et al.*, 2006) and in Anatolia (Fontugne *et al.*, 1999). This phase is likely linked to the drought event recorded at 5.2 cal kyr BP that was evidenced in the Soreq speleothem record (Bar-Matthews *et al.*, 1997) and in many others sites (Staubwasser and Weiss, 2006). The relatively wet early Holocene deduced from Lake Urmia is in contrast with the long delay in postglacial forest expansion at the beginning of the Holocene in the Southwest Asia that was pointed out by many authors (Jones and Roberts, 2008; Djamali *et al.*, 2010; Aubert *et al.*, 2019).

6. Conclusion

In this paper, we conducted systematic investigations on grain size and mineralogy of detrital and authigenic compounds that includes detailed analyses of carbonate and clays assemblages on the sedimentary sequence retrieved from the southwestern part of Lake Urmia. Our results show important changes in the lake water level for the past ~30 kyr, likely attributed to the available humidity. Although further interpretation of the hydrogeochemical characteristics and mixing processing in the lake basin is needed, the consistency of the AMS ^{14}C chronology between 22 and 2 cal kyr BP enabled us to estimate a reservoir effect for the past, which is particularly rare for such salt lakes. This reservoir age of about 2000

years has made possible to define a reliable chronology in agreement with the lithostratigraphy but also matching with the major regional environment phases.

Our work benefitted from highly reliable, precise multi-proxy data. The palaeoenvironmental reconstruction suggests a humid Late Pleistocene before the Last Glacial Maximum, followed by frequent drier/wetter episodes from that time until today, including the humid early Holocene period and evaporative conditions during the Mid to Late Holocene transition.

Being today on the eastern limit of the Mediterranean zone, NW Iran links Southern Europe, North Africa and Asia, and thus could be submitted to the respective influences of the air masses from the North Atlantic, the Indian monsoon, the Ponto-Caspian region and the Siberian anticyclone. Our results suggest that an atmospheric teleconnection existed between North Atlantic and the Western Iran during the last 30 kyr BP and will be of high interest for global understanding of climatic change in the past.

7. Acknowledgement

This work was supported by the French-Iranian project Gundishapur, the Center for International Scientific Studies and Collaboration (CISSC), TelluS Program of CNRS/INSU and China Scholarship Council (CSC).

8. References

Abbaspour, M. and Nazaridoust, A.J.I.J.o.E.S., 2007. Determination of Environmental Water Requirements of Lake Urmia, Iran: An Ecological Approach. 64(2): 161-169.

Agh, N., Van Stappen, G., Bossier, P., Sepehri, H., Lotfi, V., Rouhani, S. and Sorgeloos, P.J.P.j.o.b.s.P., 2008. Effects of Salinity on Survival, Growth, Reproductive and Life Span Characteristics of Artemia Populations from Urmia Lake and Neighboring Lagoons. 11(2): 164-172.

AghaKouchak, A., Norouzi, H., Madani, K., Mirchi, A., Azarderakhsh, M., Nazemi, A., Nasrollahi, N., Farahmand, A., Mehran, A. and Hasanzadeh, E., 2015. Aral Sea Syndrome Desiccates Lake Urmia: Call for Action. Journal of Great Lakes Research, 41(1): 307-311.

Ahmady-Birgani, H., Mirnejad, H., Feiznia, S. and McQueen, K.G., 2015. Mineralogy and Geochemistry of Atmospheric Particulates in Western Iran. Atmospheric Environment, 119: 262-272.

Ahmady-Birgani, H., Ravan, P., Schlosser, J.S., Cuevas-Robles, A., AzadiAghdam, M. and Sorooshian, A., 2020. On the Chemical Nature of Wet Deposition over a Major Desiccated Lake: Case Study for Lake Urmia Basin. Atmospheric Research, 234.

Alderman, A. and Skinner, H.C.W.J.A.J.o.S., 1957. Dolomite Sedimentation in the South-East of South Australia. 255(8): 561-567.

Alderman, A. and Von Der Borch, C.J.N., 1960. Occurrence of Hydromagnesite in Sediments in South Australia. 188(4754): 931-931.

Alderman, A. and Von der Borch, C.J.N., 1961. Occurrence of Magnesite–Dolomite Sediments in South Australia. 192(4805): 861-861.

Alderman, A. and Von der Borch, C.J.N., 1963. A Dolomite Reaction Series. 198(4879): 465-466.

Alipour, S., 2006. Hydrogeochemistry of Seasonal Variation of Urmia Salt Lake, Iran. Saline Syst, 2: 9. Available from https://www.ncbi.nlm.nih.gov/pubmed/16834770.

Asem, A., Mohebbi, F. and Ahmadi, R.J.W.a., 2012. Drought in Urmia Lake, the Largest Natural Habitat of Brine Shrimp Artemia. 43(1): 36-38.

Aubert, C., Brisset, E., Djamali, M., Sharifi, A., Ponel, P., Gambin, B., Akbari Azirani, T., Guibal, F., Lahijani, H. and Naderi Beni, A.J.J.o.P., 2017. Late Glacial and Early Holocene Hydroclimate Variability in Northwest Iran (Talesh Mountains) Inferred from Chironomid and Pollen Analysis. 58(2): 151-167.

Aubert, C., Djamali, M., Jones, M., Lahijani, H., Marriner, N., Naderi-Beni, A., Sharifi, A., Ponel, P. and Gandouin, E.J.C.j.o.e.s., 2019. A Major Hydrobiological Change in Dasht-E Arjan Wetland (Southwestern Iran) During the Late Glacial–Early Holocene Transition Revealed by Subfossil Chironomids. 56(8): 848-856.

Bar-Matthews, M., Ayalon, A. and Kaufman, A.J.Q.R., 1997. Late Quaternary Paleoclimate in the Eastern Mediterranean Region from Stable Isotope Analysis of Speleothems at Soreq Cave, Israel. 47(2): 155-168.

Bottema, S., 1986. A Late Quaternary Pollen Diagram from Lake Urmia (Northwestern Iran). Review of Palaeobotany and Palynology, 47(3-4): 241-&. Available from <Go to ISI>://WOS:A1986C797800004 https://www.sciencedirect.com/science/article/abs/pii/0034666786900394?via%3Dihub.

Chamley, H., 1989. Clay Mineralogy.

Clayton, R.N. and Jones, B.F.J.G.e.C.A., 1968. Isotope Studies of Dolomite Formation under Sedimentary Conditions. 32(4): 415-432.

Curtis, C., 1987. Mineralogical Consequences of Organic Matter Degradation in Sediments: Inorganic/Organic Diagenesis. In: Marine Clastic Sedimentology. Springer: pp: 108-123.

Diekmann, B., Petsehick, R., Gingele, F., Fütterer, D., Abelmann, A., Brathauer, U., Gersonde, R. and Mackensen, A., 1996. Clay Mineral Fluctuations in Late Quaternary Sediments of the Southeastern South Atlantic: Implications for Past Changes of Deep Water Advection. In: The South Atlantic. Springer: pp: 621-644.

Djamali, M., de Beaulieu, J.-L., Shah-hosseini, M., Andrieu-Ponel, V., Ponel, P., Amini, A., Akhani, H., Leroy, S.A.G., Stevens, L., Lahijani, H. and Brewer, S., 2008a. A Late Pleistocene Long Pollen Record from Lake Urmia, Nw Iran. Quaternary Research, 69(03): 413-420.

Djamali, M., Kürschner, H., Akhani, H., de Beaulieu, J.-L., Amini, A., Andrieu-Ponel, V., Ponel, P. and Stevens, L., 2008b. Palaeoecological Significance of the Spores of the Liverwort Riella (Riellaceae) in a Late Pleistocene Long Pollen Record from the Hypersaline Lake Urmia, Nw Iran. Review of Palaeobotany and Palynology, 152(1-2): 66-73.

Djamali, M., Ponel, P., Delille, T., Thiéry, A., Asem, A., Andrieu-Ponel, V., de Beaulieu, J.-L., Lahijani, H., Shah-Hosseini, M. and Amini, A.J.I.J.o.A.S., 2010. A 200,000-Year Record of the Brine Shrimp Artemia (Crustacea: Anostraca) Remains in Lake Urmia, Nw Iran. 1(1): 14-18.

Eastwood, W.J., Leng, M.J., Roberts, N. and Davis, B.J.J.o.Q.S.P.f.t.Q.R.A., 2007. Holocene Climate Change in the Eastern Mediterranean Region: A Comparison of Stable Isotope and Pollen Data from Lake Gölhisar, Southwest Turkey. 22(4): 327-341.

Ehrmann, W., Setti, M. and Marinoni, L., 2005. Clay Minerals in Cenozoic Sediments Off Cape Roberts (Mcmurdo Sound, Antarctica) Reveal Palaeoclimatic History. Palaeogeography, Palaeoclimatology, Palaeoecology, 229(3): 187-211.

Erfan, S., Rezaei, K., Lak, R. and Aleali, S.M., 2017. Clay Mineralogy and Sediment Grain-Size Variations as Climatic Signals in Southern Part of Urmia Lake Cores, North West of Iran.

Esmaeili Dahesht, L., Negarestan, H., Eimanifar, A., Mohebbi, F. and Ahmadi, R.J.I.J.o.F.S., 2010. The Fluctuations of Physicochemical Factors and Phytoplankton Populations of Urmia Lake, Iran. 9(3): 361-381.

Esquevin, J.J.B.C.R.P.-S., 1969. Influence De La Composition Chimique Des Illites Sur Leur Cristallinité. 3(1): 147-153.

Eugster, H., Kelts, K.J.C.s. and geomorphology, 1983. Lacustrine Chemical Sediments. 321-368.

Eugster, H.P. and Jones, B.F.J.A.j.o.s., 1979. Behavior of Major Solutes During Closed-Basin Brine Evolution. 279(6): 609-631.

Fontes, J.-C., Gasse, F. and Gibert, E.J.P., Palaeoclimatology, Palaeoecology, 1996. Holocene Environmental Changes in Lake Bangong Basin (Western Tibet). Part 1: Chronology and Stable Isotopes of Carbonates of a Holocene Lacustrine Core. 120(1-2): 25-47.

Fontes, J.C., Mélières, F., Gibert, E., Qing, L. and Gasse, F.J.Q.S.R., 1993. Stable Isotope and Radiocarbon Balances of Two Tibetan Lakes (Sumxi Co, Longmu Co) from 13,000 Bp. 12(10): 875-887.

Fontugne, M., Kuzucuoğlu, C., Karabiyikoğlu, M., Hatte, C. and Pastre, J.-F.J.Q.S.R., 1999. From Pleniglacial to Holocene: A 14c Chronostratigraphy of Environmental Changes in the Konya Plain, Turkey. 18(4-5): 573-591.

Gasse, F.J.Q.S.R., 2000. Hydrological Changes in the African Tropics since the Last Glacial Maximum. 19(1-5): 189-211.

Ghalibaf, M.B. and Moussavi, Z.J.E.J.o.S.D., 2014. Development and Environment in Urmia Lake of Iran. 3(3): 219-219.

Hua, Q., Turnbull, J.C., Santos, G.M., Rakowski, A.Z., Ancapichún, S., De Pol-Holz, R., Hammer, S., Lehman, S.J., Levin, I. and Miller, J.B.J.R., 2021. Atmospheric Radiocarbon for the Period 1950–2019. 1-23.

Jalali, B., Sicre, M.-A., Bassetti, M.-A. and Kallel, N.J.C.o.t.P., 2016. Holocene Climate Variability in the North-Western Mediterranean Sea (Gulf of Lions). 12(1): 91-101.

Jones, M.D., Roberts, C.N. and Leng, M.J.J.Q.R., 2007. Quantifying Climatic Change through the Last Glacial–Interglacial Transition Based on Lake Isotope Palaeohydrology from Central Turkey. 67(3): 463-473.

Jones, M.D. and Roberts, C.N.J.Q.i., 2008. Interpreting Lake Isotope Records of Holocene Environmental Change in the Eastern Mediterranean. 181(1): 32-38.

Kelts, K. and Shahrabi, M., 1986. Holocene Sedimentology of Hypersaline Lake Urmia, Northwestern Iran. %J Palaeogeography, Palaeoclimatology, Palaeoecology, 54(1-4): 105-130.

Kuzucuoğlu, C., Christol, A., Mouralis, D., Doğu, A.F., Akköprü, E., Fort, M., Brunstein, D., Zorer, H., Fontugne, M. and Karabiyikoğlu, M.J.J.o.Q.S., 2010. Formation of the Upper Pleistocene Terraces of Lake Van (Turkey). 25(7): 1124-1137.

Landmann, G., Reimer, A., Lemcke, G. and Kempe, S.J.P., Palaeoclimatology, Palaeoecology, 1996. Dating Late Glacial Abrupt Climate Changes in the 14,570 Yr Long Continuous Varve Record of Lake Van, Turkey. 122(1-4): 107-118.

Lippmann, F., 1973. Crystal Chemistry of Sedimentary Carbonate Minerals. In: Sedimentary Carbonate Minerals. Springer: pp: 5-96.

McKenzie, D., 1976. The East Anatolian Fault: A Major Structure in Eastern Turkey. 29(1): 189-193.

Mirzapour, B., Lak, R., Aleali, M., Djamali, M. and Shahbazi, R., 2021a. Mineralogical Reconstruction of Late Pleistocene - Holocene Climate and Environmental Changes in Southern Wetlands of Lake Urmia. Geopersia, 11(1): 205-218. Available from <Go to ISI>://WOS:000658392900011.

Mirzapour, B., Lak, R., Aleali, M., Djamali, M. and Shahbazi, R.J.P., 2021b. Identifying the Effects of Climate Changes on Sedimentary Environments and Determining the Sedimentation Rate of South Wetlands of Lake Urmia During Late Pleistocene and Holocene. 7(1): 113-127.

Müller, G., Irion, G. and Förstner, U.J.N., 1972. Formation and Diagenesis of Inorganic Ca-Mg Carbonates. 59: 158-164.

Pengra, B.J.U.-G., Sioux Falls, UNEP Global Environmental Alert Service, 2012. The Drying of Iran's Lake Urmia and Its Environmental Consequences.

Peterson, M., Bien, G. and Berner, R.J.J.o.G.R., 1963. Radiocarbon Studies of Recent Dolomite from Deep Spring Lake, California. 68(24): 6493-6505.

Peterson, M. and Bien, G.J.A.J.o.S., 1966. Growth of Dolomite Crystals. 264(4): 257-272.

Pierre, C., Ortlieb, L. and Person, A.J.J.o.S.R., 1984. Supratidal Evaporitic Dolomite at Ojo De Liebre Lagoon; Mineralogical and Isotopic Arguments for Primary Crystallization. 54(4): 1049-1061.

Post, F. and Youssef, N.J.C.J.o.M., 1977. A Procaryotic Intracellular Symbiont of the Great Salt Lake Brine Shrimp Artemia Salina (L.). 23(9): 1232-1236.

Reimer, P.J., Austin, W.E., Bard, E., Bayliss, A., Blackwell, P.G., Ramsey, C.B., Butzin, M., Cheng, H., Edwards, R.L. and Friedrich, M.J.R., 2020. The Intcal20 Northern Hemisphere Radiocarbon Age Calibration Curve (0–55 Cal Kbp). 62(4): 725-757.

Reimer, P.J., Bard, E., Bayliss, A., Beck, J.W., Blackwell, P.G., Ramsey, C.B., Buck, C.E., Cheng, H., Edwards, R.L. and Friedrich, M.J.r., 2013. Intcal13 and Marine13 Radiocarbon Age Calibration Curves 0–50,000 Years Cal Bp. 55(4): 1869-1887.

Roberts, N., Jones, M., Benkaddour, A., Eastwood, W., Filippi, M., Frogley, M., Lamb, H., Leng, M., Reed, J. and Stein, M.J.Q.S.R., 2008. Stable Isotope Records of Late Quaternary Climate and Hydrology from Mediterranean Lakes: The Isomed Synthesis. 27(25-26): 2426-2441.

Roberts, N., Reed, J., Leng, M., Kuzucuoğlu, C., Fontugne, M., Bertaux, J., Woldring, H., Bottema, S., Black, S. and Hunt, E.J.T.H., 2001. The Tempo of Holocene Climatic Change in the Eastern Mediterranean Region: New High-Resolution Crater-Lake Sediment Data from Central Turkey. 11(6): 721-736.

Sharifi, A., Pourmand, A., Canuel, E.A., Ferer-Tyler, E., Peterson, L.C., Aichner, B., Feakins, S.J., Daryaee, T., Djamali, M. and Beni, A.N.J.Q.S.R., 2015. Abrupt Climate Variability since the Last Deglaciation Based on a High-Resolution, Multi-Proxy Peat Record from Nw Iran: The Hand That Rocked the Cradle of Civilization? , 123: 215-230.

Sharifi, A., Shah-Hosseini, M., Pourmand, A., Esfahaninejad, M. and Haeri-Ardakani, O., 2018. The Vanishing of Urmia Lake: A Geolimnological Perspective on the Hydrological Imbalance of the World's Second Largest Hypersaline Lake.

Shumilovskikh, L.S., Fleitmann, D., Nowaczyk, N., Behling, H., Marret, F., Wegwerth, A. and Arz, H.W.J.C.o.t.P., 2014. Orbital-and Millennial-Scale Environmental Changes between 64 and 20 Ka Bp Recorded in Black Sea Sediments. 10(3): 939-954.

Skinner, H.C.W.J.A.J.o.S., 1963. Precipitation of Calcian Dolomites and Magnesian Calcites in the Southeast of South Australia. 261(5): 449-472.

Staubwasser, M. and Weiss, H.J.Q.R., 2006. Holocene Climate and Cultural Evolution in Late Prehistoric–Early Historic West Asia. 66(3): 372-387.

Stevens, L.R., Djamali, M., Andrieu-Ponel, V. and de Beaulieu, J.-L., 2012. Hydroclimatic Variations over the Last Two Glacial/Interglacial Cycles at Lake Urmia, Iran. Journal of Paleolimnology, 47(4): 645-660.

Stevens, L.R., Ito, E., Schwalb, A. and Wright, H.E.J.Q.r., 2006. Timing of Atmospheric Precipitation in the Zagros Mountains Inferred from a Multi-Proxy Record from Lake Mirabad, Iran. 66(3): 494-500.

Stuiver, M., Reimer, P. and Reimer, R., 2021. Calib 8.2 [Www Program] at Http://Calib. Org. Accessed.

Talebi, T., Ramezani, E., Djamali, M., Lahijani, H.A.K., Naqinezhad, A., Alizadeh, K. and Andrieu-Ponel, V.J.Q.I., 2016. The Late-Holocene Climate Change, Vegetation Dynamics, Lake-Level Changes and Anthropogenic Impacts in the Lake Urmia Region, Nw Iran. 408: 40-51.

Tudryn, A., Motavalli-Anbaran, S.-H., Tucholka, P., Gibert-Brunet, E., Lankarani, M., Ahmady-Birgani, H., Kong, T., Noret, A., Miska, S., Massault, M. and Dufaure, O., 2021. Late Quaternary Environmental Changes of Lake Urmia Basin (Nw Iran) Inferred from Sedimentological and Magnetic Records. Quaternary International, 589: 83-94.

Von der Borch, C. and Jones, J.J.S., 1976. Spherular Modern Dolomite from the Coorong Area, South Australia. 23(4): 587-591.

von Der Borch, C.J.G.e.C.A., 1965. The Distribution and Preliminary Geochemistry of Modem Carbonate Sediments of the Coorong Area, South Australia. 29(7): 781-799.

Wasylikowa, K., Witkowski, A., Walanus, A., Hutorowicz, A., Alexandrowicz, S.W. and Langer, J.J.J.Q.R., 2006. Palaeolimnology of Lake Zeribar, Iran, and Its Climatic Implications. 66(3): 477-493.

Wurtsbaugh, W.A. and Gliwicz, Z.M., 2001. Limnological Control of Brine Shrimp Population Dynamics and Cyst Production in the Great Salt Lake, Utah. In: Saline Lakes. Springer: pp: 119-132.

Figure captions

Fig. 1 Lake Urmia: (a) location of the lake and lake's catchment area, black rectangle indicates study area; (b) simplified geological map of Lake Urmia catchment area (after Sharifi et al., 2018, completed with information from Geological Map of Iran, Sheet No 1 Nort-West Iran); (c) detailed geological map of the study area with location of samples from the catchment area (1 to 8) and of coring site (G). Lithological units: pCmt1 - Medium grade (Amphibolite Facies) Precambrian metamorphic; pCmt2 – Low grade , regional metamorphic rocks (Green Schist Facies); Jph - Phyllite, slate and meta-sandstone (Hamadan Phyllites); Omrb - Red Beds composed of red conglomerate, sandstone, marl; Qft1 - High level piedmont fan and valley terraces deposits; Omql – Massive to thick - bedded reefal limestone; Pr - Dark grey medium - bedded to massive limestone (RUTEH); Qsl - Clay flate; Qt3 - no description – lake; Pmlb1 - Pyroclastics and claystone with vertebrate fauna remains; Pcr - Dolomite , sandstone and volcanic rocks (Rizu Series); Pck :Dull green grey slaty shales.

Fig. 2 Down-core variation of simplified lithofacies from Lake Urmia sediments: (a) core Golman 6; (b) core Golman 7; (c) composite core and lithology units, optical microphotograph from composite core for: (d) clay at 12.12 m depth; (e) fine silt at 4.12 m depth; (f) sand at 2.75 m depth; (g) clayish sediment with fecal pellets at 10.92 m depth; (h) fecal pellet rich clayish sediment at 3.09 m depth; (i) sandy sediment with fecal pellet rich at 2.00 m depth.

Fig. 3 Down-core variation in lithology and in grain size distribution of Lake Urmia sediments and of catchment samples (grey squares numbered from 1 to 8).

Fig. 4 Down-core variation in lithology and in total mineralogy of Lake Urmia sediments and of catchment samples (grey squares numbered from 1 to 8) with percentages of minerals in (a), (b), (c), (d), (e), (f), (h), (j), and mineral crystallinity index in (g) (i) (k).

Fig. 5 Down-core variation in lithology and in clay mineral composition of Lake Urmia sediments and of catchment samples (grey squares numbered from 1 to 8) with percentages of clay minerals in (a), (b), (c), (d), smectite and illite crystallinity index in (e), (f), and illite chemistry in (g).

Fig. 6 Evolution of sedimentological parameters against a ^{14}C time scale: (a) magnetic susceptibility (susc.), (b) clay fraction (%), (c) mean grain size (μm), (d) smectite/illite ratio, (e) illite crystallinity (crys.), (f) quartz percentage (%), (g) evaporate percentage (%), (h) carbonate and aragonite percentages (%), (i) dolomite crystallinity(crys.), and (j) NGRIP curve (reference).

Table captions

Table 1 Location and description of Lake Urmia cored sequences and of geological samples from the Shahr Chay River catchment. Numbering of cores and samples in the text and figures refers to this table.

Table 2 AMS-^{14}C calibrated ages of Lake Urmia sediments. Sample depth refers to the composite core (see text). All corrections and calibration are detailed in paragraph "^{14}C chronology".

Table 3 Mineralogy including crystallinity of selected minerals, and grain-size parameters on the geological samples collected from the Shahr Chay River catchment.

Figure 1

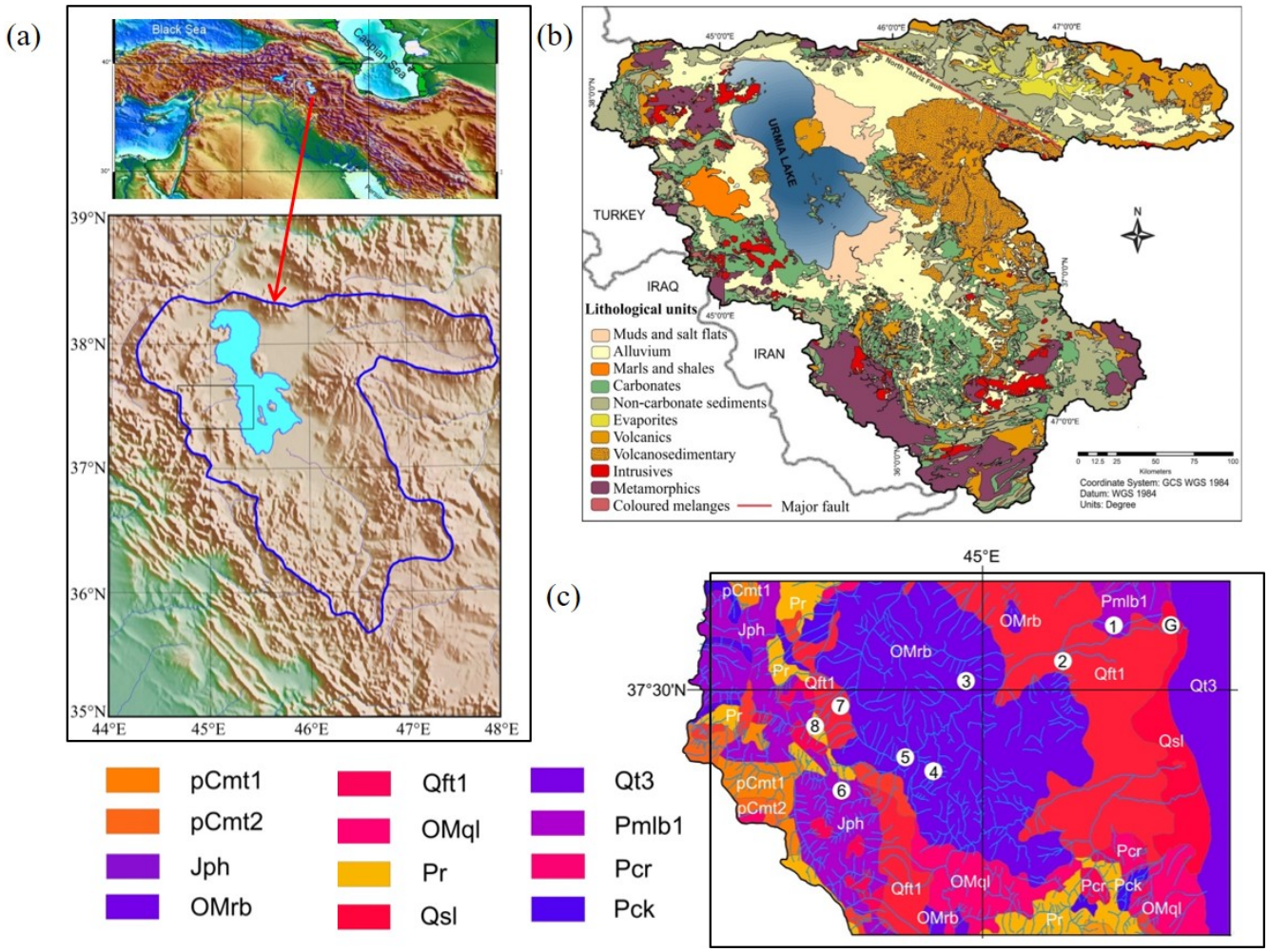
(a)
Black Sea
Caspian Sea
39°N
38°N
37°N
36°N
35°N
44°E
45°E
46°E
47°E
48°E
(b)
URMIA LAKE
TURKEY
IRAQ
IRAN
Lithological units
Muds and salt flats
Alluvium
Marls and shales
Carbonates
Non-carbonate sediments
Evaporites
Volcanics
Volcanosedimentary
Intrusives
Metamorphics
Coloured melanges
Major fault
Coordinate System: GCS WGS 1984
Datum: WGS 1984
Units: Degree
(c)
45°E
37°30'N
pCmt1
pCmt2
Jph
OMrb
Qft1
OMql
Pr
Qsl
Qt3
Pmlb1
Pcr
Pck

Figure 2

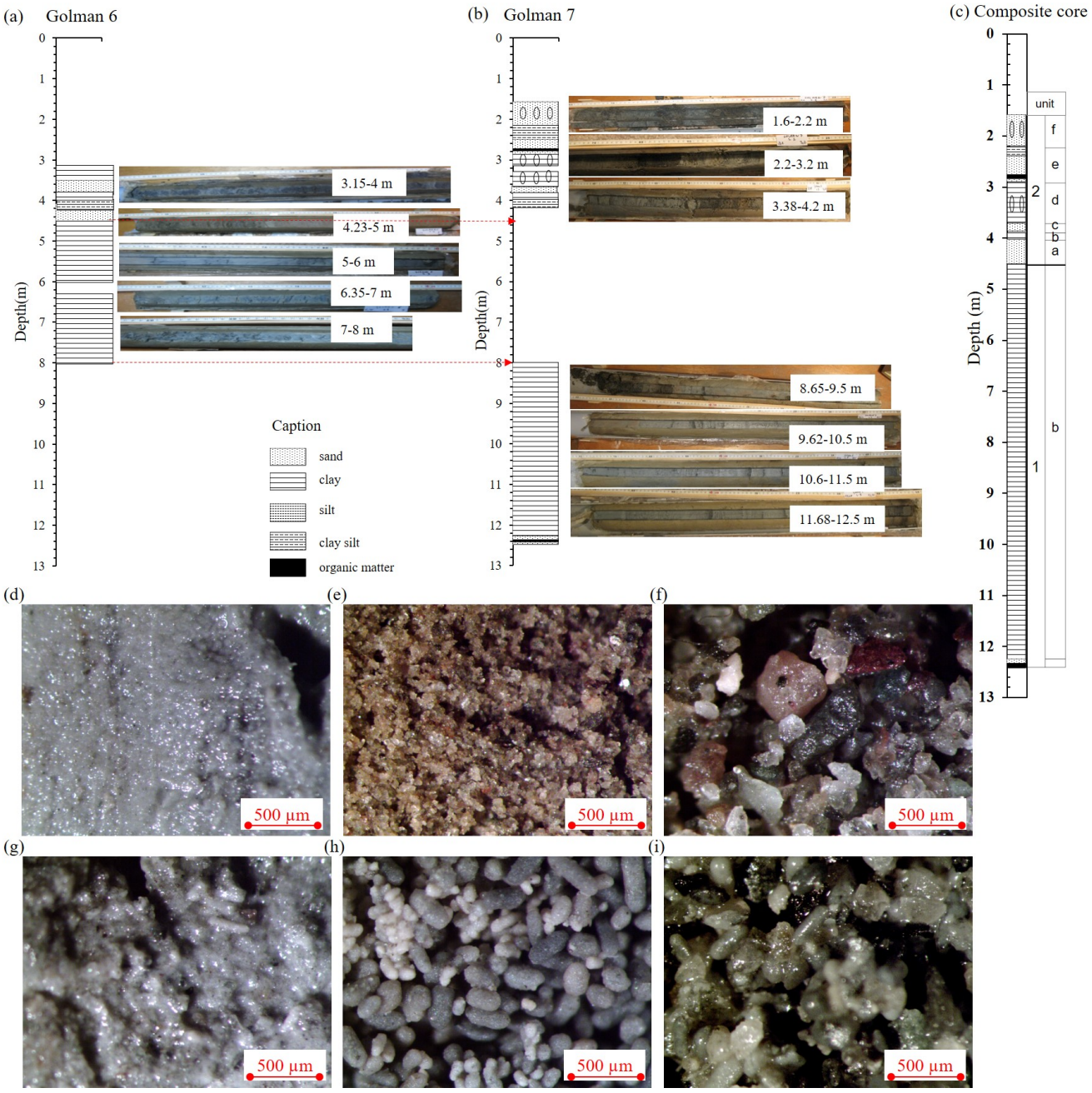
(a) Golman 6
(b) Golman 7
(c) Composite core
Depth(m)
Depth (m)
3.15-4 m
4.23-5 m
5-6 m
6.35-7 m
7-8 m
1.6-2.2 m
2.2-3.2 m
3.38-4.2 m
8.65-9.5 m
9.62-10.5 m
10.6-11.5 m
11.68-12.5 m
Caption
sand
clay
silt
clay silt
organic matter
unit
f
e
d
c
b
a
2
1
b
(d)
(e)
(f)
(g)
(h)
(i)
500 µm

Figure 3

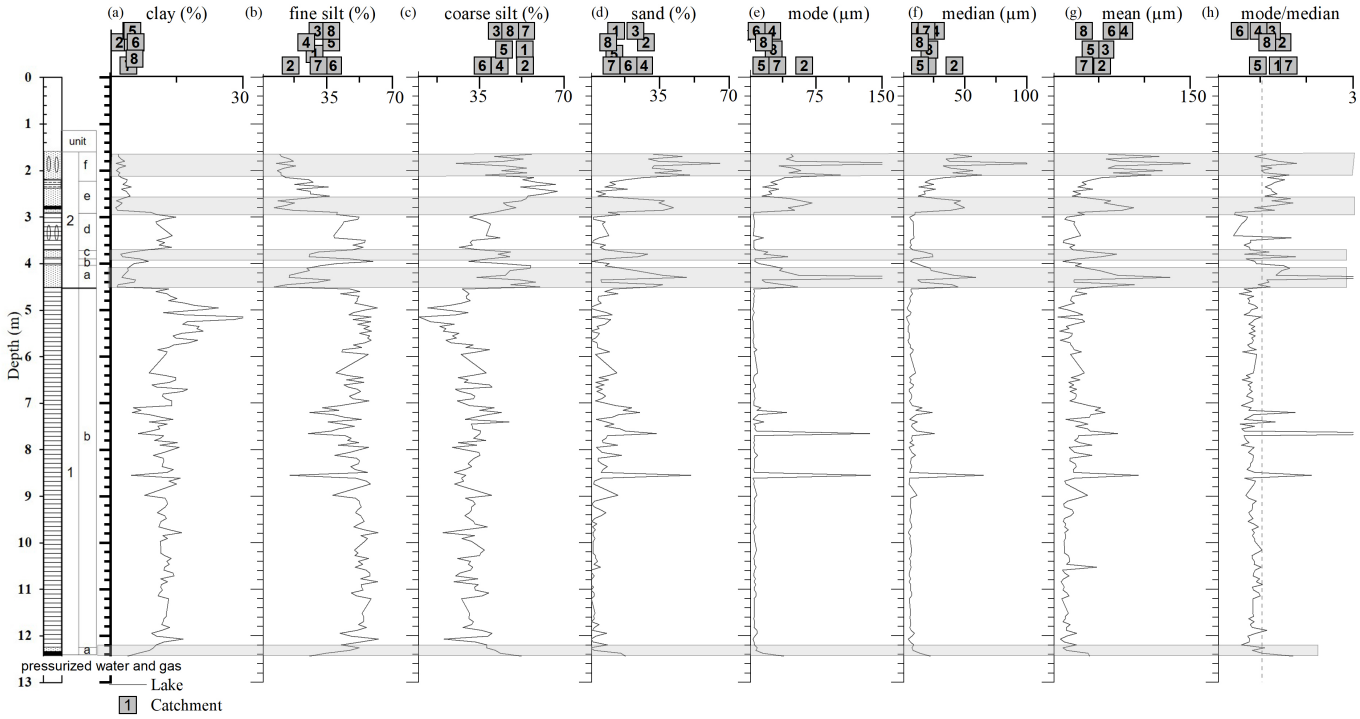

Figure 4

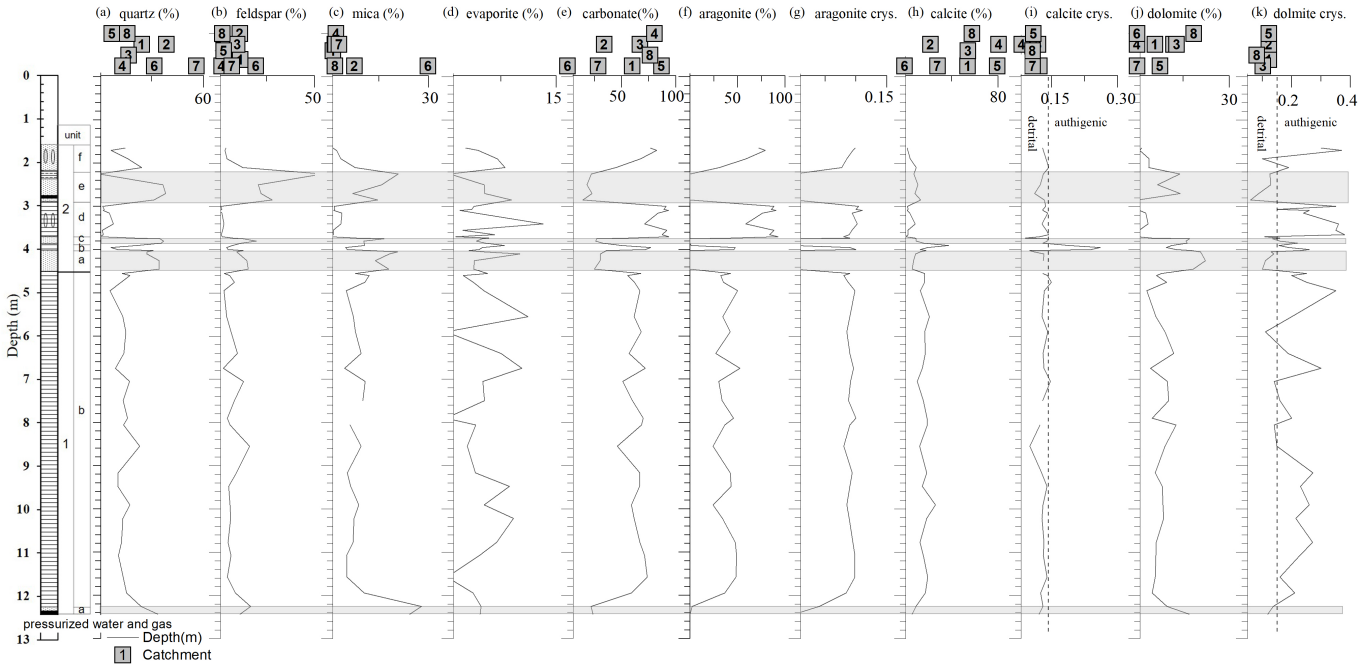

Figure 5

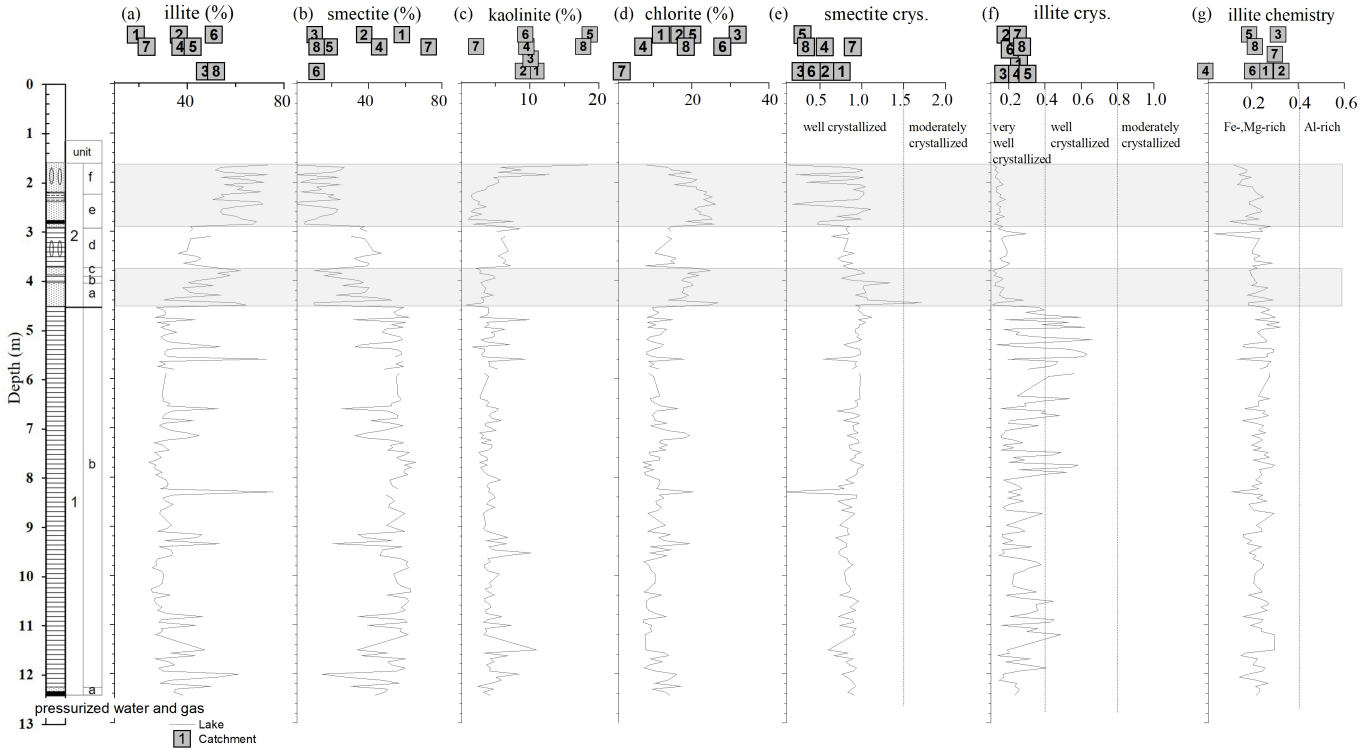

Figure 6

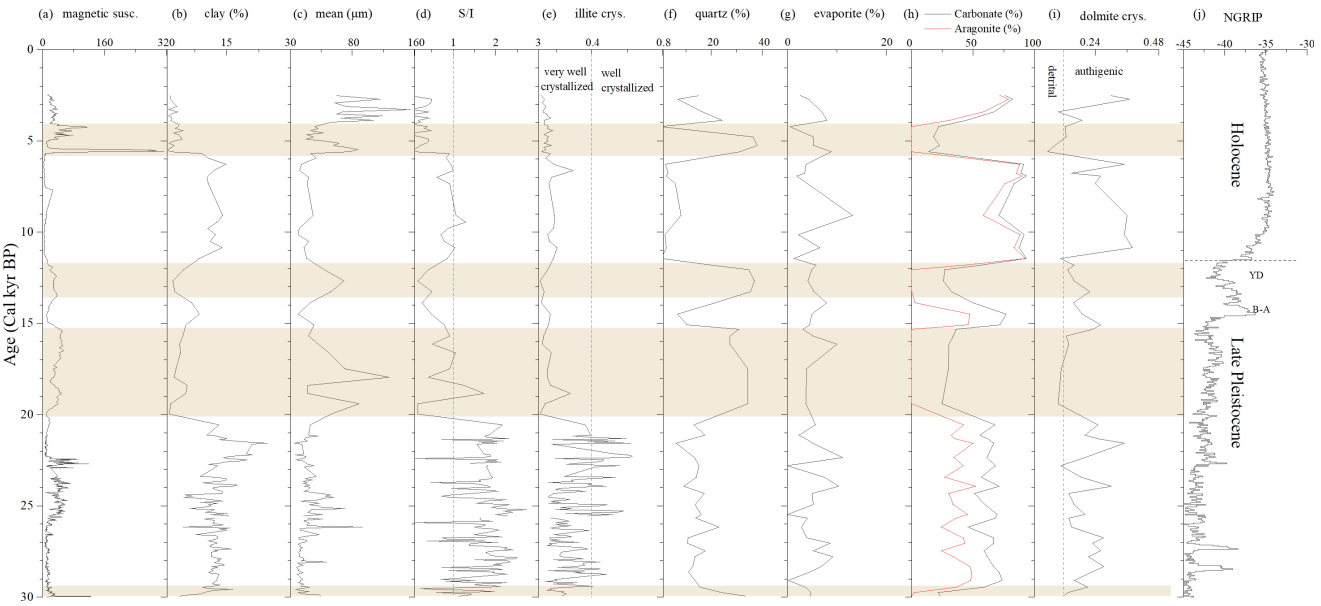

Table 1

	Site name	Comment on sampling	Latitude N	Longitude E	Altitude m asl ±1 m
Coring well	Golman 6	8 m deep	37°35′28.854″	45°16′33.834″	1270
	Golman 7	12.5 m deep	37°35′28.746″	45°16′33.75″	1270
Catchment area samples	1	Pyroclastic and claystone with vertebrate fauna remains, andesitic to basaltic volcanics	37°34'48"	45°12'00"	1370
	2	High level piedmont fan and valley terraces deposits	37°32'24"	45°07'12"	1311
	3	Red Beds composed of red conglomerate, sandstone, marl, gypsiferous marl (mostly limestones)	37°28'48"	44°57'36"	1484
	4	Red Beds composed of red conglomerate, sandstone, marl, gypsiferous marl (pure marl)	37°23'24"	44°55'12"	1720
	5	Red Beds composed of red conglomerate, sandstone, marl, gypsiferous marl	37°24'36"	44°52'48"	1614
	6	Phyllite, slate and meta-sandstone (Hamadan Phyllites)	37°22'12"	44°48'00"	2820
	7	High level piedmont fan and valley terraces deposits	37°28'48"	44°47'24"	1788
	8	Dark gray medium- bedded to massive limestone (limestone)	37°27'00"	44°45'00"	2246

Table 2

Sample	Depth (cm)	Type (*)	Sample Nr	$F^{14}C$ (pMC)	σ (b)	Measured ^{14}C ages (BP)	σ (b)	Mineralogy of the carbonate fraction Aragonite (%)	Calcite (%)	Dolomite (%)	Crystallinity of the carbonate fraction Aragonite	Calcite	Dolomite	$\delta^{13}C$ (‰ PDB)(c)
Lake surface water			E2476	93,46	0,250	540	20							-1,10
Golman-5 core														
G5	2,34	Charcoal	B2087	0,5824	0,20	4 343	25							-14,50
G5	2,66	Charcoal	B2088	0,5787	0,20	4 394	22							-25,50
Composite core (Golman-6 and Golman-7 cores)														
G7	1,70	$CaCO_3$		0,5580	0,32	4 265	26	94,2	3,8	1,9	0,131	***0,095***	0,370	
G7	1,85	OM	B2295	0,5306	0,002	5 090	25							
G7-S2	2.80	Charcoal	B2097	0,5547	0,40	4 735	22							-26,50
G7-S2	3,07	$CaCO_3$	CaCO3	0,3334	0,42	8 825	34	95,9	3,3	0,7	0,100	***0,130***	***0,150***	
G7-S2	3,09	White FP (**)	A21542	0,3666	0,0035	8060	80	100.0						
G7-S2	3,09	Black FP (**)	A21543	0,3880	0,0036	7600	80	(secondary carbonate precipitation suspected)						
G7-S2	3,09	$CaCO_3$	CaCO3	0,3579	0,41	8 250	33	96,7	2,3	<0,01	0,110	***0,130***	0,230	
G7-S3	3,65	$CaCO_3$	CaCO3	0,2377	0,53	11 540	42	93,9	4,2	1,8	0,143	***0,089***	0,380	
G7	4,05	OM	B2297	0,1529	0,10	15 090	66							-25,3
G6-S2	4,40	OM	B2304	0,1124	0,0011	17 560	76							
G6 S2	4,60	$CaCO_3$	62001	0,0662	0,12	21 810	140	58,3	30,2	11,4	0,100	***0,140***	0,200	
G6-S4	6,45	OM	B2300	0,0689	0,0005	21 490	63							
G7 S6b	8,85	OM	B2099	0,0554	0,12	23 240	170	51,3	21,1	25,7		***0,123***	***0,140***	
G7-S8	12.46	Charcoal	B2301	0,0005	0,001	25 590	96							-25,90

Sample	Depth (cm)	Type (a)	Sample Nr	$F^{14}C$ (pMC)	σ (b)	Measured ^{14}C ages	σ (b)	^{14}C Ages corrected from detrital fraction (yr BP)	^{14}C Ages corrected from a 2-kyr HWE (yr BP)	Calibrated ^{14}C Ages (cal BP)	2σ
Lake surface water		Water	E2476	93,46	0,250	540	20				
Golman-5 core											
G5	2,34	Charcoal	B2087	0,5824	0,20	4 343	25	4 340	4 340	**4 910**	-60/+60
G5	2,66	Charcoal	B2088	0,5787	0,20	4 394	22	4 390	4 390	**4 940**	-75/+100
Composite core (Golman-6 and Golman-7 cores)											
G7	1,70	$CaCO_3$		0,5580	0,320	4 265	26	**4 560**	2 560	**2 720**	-205/+30
G7	1,85	OM	B2295	0,5306	0,002	5 090	25	3 090	3 090	**3 295**	-75/+65
G7-S2	2.80	Charcoal	B2097	0,5547	0,400	4 735	22	4 730	4 730	**5 475**	-145/+105
G7-S2	3,07	$CaCO_3$	CaCO3	0,3334	0,420	8 825	34	**8 730**	6 730	7 595	-80/+70
G7-S2	3,09	Black FP (**)	A21543	0,3880	0,0036	7 600	80	*(secondary carbonate precipitation suspected)*			
G7-S2	3,09	White FP (**)	A21542	0,3666	0,0035	8 060	80	8 060	6 060	**6 920**	-180/+240
G7-S2	3,09	$CaCO_3$	CaCO3	0,3579	0,410	8 300	33	**8 300**	6 300	7 215	-55/+90
G7-S3	3,65	$CaCO_3$	CaCO3	0,2377	0,530	11 540	42	**11 520**	9 520	**10 850**	-245/+225
G7-S3	4,05	OM	B2297	0,1529	0,100	15 090	66	15 090	13 090	**15 695**	-230/+235
G6-S2	4,40	OM	B2304	0,1124	0,0011	17 560	76	17 560	15 560	**18 845**	-135/+135
G6-S2	4,60	$CaCO_3$	62001	0,0662	0,120	21 810	140	**19 470**	17 470	**21 115**	-385/+575
G6-S4	6,45	OM	B2300	0,0689	0,0005	21 490	63	19 490	17 490	**23 510**	-260/+255
G7 S6b	8,85	OM	B2099	0,0830	0,123	23 240	82	23 240	21 240	**25 610**	-555/+375
G7-S8	12.46	Charcoal	B2301	0,0005	0,001	25 590	96	25 590	25 590	**29 950**	-290/+165

(*) Apparent Hard Water Effect (HWE) calculated with a ^{14}C activity of atmosphere of 100 pMC
(a) CaCO3: total carbonate fraction; OM: diffused organic matter; FP: fecal pellets (*Artemia*)
(b) Error bars represent one sigma deviation
(c) Accuracies on ^{13}C measurements are of ±0.05 and ±0.02% PDB for carbonates and organic matter, respectively
(d) *Stuiver, M., Reimer, P.J., and Reimer, R.W., 2021, CALIB 8.2 [WWW program] at http://calib.org*